# UNIVERSIDAD DE CONCEPCIÓN

## FACULTAD DE INGENIERÍA

### DEPARTAMENTO DE INGENIERÍA ELÉCTRICA

# MODELING AND CONTROL OF MICRO CHANNEL THROUGH PORT HAMILTONIAN SYSTEMS (PHS)

Tesis presentada a la Facultad de Ingeniería de la Universidad de Concepción para optar al grado académico de Magíster en Ciencias de la Ingeniería con mención en Ingeniería Eléctrica


POR: Nelson Eduardo Cisneros Pinto

Profesor Guía: PhD. Alejandro José Rojas Norman

Profesor Co-Guía: PhD. Héctor Miguel Ramírez Estay



Concepción, Chile 2020

# ABSTRACT

Flood control and water supply are important aspects that can improve the life quality of many people. Saint Venant equations are one of the most popular models used by hydraulic engineers to express the behavior of open channel flows. The problem with the models based on Saint Venant equations are that they are difficult to analyze and simulate.

The micro-channel is an experimental plant that can represent open channel flow hydraulic phenomena at scale.

We propose in this thesis the model of a micro-channel using a port-Hamiltonian system approach. The model is represented by a series of tanks and pipes interconnected in series. These hydraulic elements can be interpreted as basic elements equivalent to electric components such as capacitors, inductance and resistors.With the basic element structure established tank+pipe an identification experiment was done to identify the Port-Hamiltonian System (PHS) model parameters. We use Ordinary Least Square (OLS) to adjust the model to the experimental setup.

Based on the interconnected model a controller was designed using the total hydraulic-mechanical energy as a local Lyapunov function. The objective is to control the water height level inside the micro-channel.

Due to the micro-channel model and the model gate errors an Integral Action Controller (IAC) was designed. The controller based on the total hydraulic-mechanical energy as a local Lyapunov function shows good simulation results but presents steady state error in the experimental results. The IAC shows good simulated and experimental results even with an input flow perturbation.

# ACKNOWLEDGEMENTS

I want to thank SENESCYT (Secretaría de Educación Superior, Ciencia, Tecnología e Innovación, Ecuador) for its financial support. I thank my supervisors for their guidance in the development of this work. This assignment could not be completed without the cooperation of my laboratory partners.

Last but not the least I would like to thank my Chilean friends, my family especially to my grandfather for being a source of inspiration to me.

# CONTENTS

# LIST OF FIGURES

# LIST OF TABLES

# SYMBOLS

| | | |
|---|---|---|
| $V$ | :Volume | $(m^3)$ |
| $\Pi$ | :Momentum | $(Ns/m^2)$ |
| $q$ | :Flow | $(m^3/s)$ |
| $p$ | :Pressure | $(N/m^2)$ |
| $p_{ext}$ | :External pressure | $(N/m^2)$ |
| $p_{\Delta}$ | :Slope drop pressure | $(N/m^2)$ |
| g | :Gravity | $(m^2/s)$ |
| $H_d$ | :Desired energy | $(J)$ |
| $H_{cl}$ | :Closed-loop energy | $(J)$ |
| $H_c$ | :Control energy | $(J)$ |
| $u$ | :Control signal | $(Ns/m^5)$ |
| $u_c$ | :Controller input | $(m^3/s)$ |
| $y$ | :Model output | $(m^3/s)$ |
| $y_c$ | :Controller output | $(N/m^2)$ |
| $\mathrm{d}_1$ | :Matched disturbance | $(N/m^2)$ |
| $\mathrm{d}_2$ | :Unmatched disturbance | $(m^3/s)$ |
| $W$ | :Lyapunov candidate | $(J)$ |
| $w$ | :State vector | |

| | | |
|---|---|---|
| $\alpha, \beta, \delta, \mathrm{R_a}, \mathrm{I_a}$ | :Controller constants | |
| $\zeta, z$ | :Controller state | |
| $\hat{u}$ | :Adjusted fluid resistance | $(Ns/m^5)$ |
| $\mathrm{R_f}$ | :Uncontrolled fluid resistance | $(Ns/m^5)$ |
| $\mathrm{C_f}$ | :Fluid capacitance | $(m^5/N)$ |
| I | :Fluid inertance | $(Ns^2/m^5)$ |
| A | :Area | $(m^2)$ |
| B | :Channel width | $(m)$ |
| $h$ | :Water level height | $(m)$ |
| $\alpha_g$ | :Gate flow coefficient | |
| $\gamma, \mathrm{K_1}$ | :Model parameters | |
| $\eta$ | :Adjusted resistance parameter | |
| $\rho$ | :Fluid density | $(Kg/m^3)$ |
| $k$ | :Sample-indexing variable | |
| $\mathrm{T_s}$ | :Sample period | $(s)$ |
| $m, n$ | :Dimensions | |

The none italic letters represent constants.

# 1. INTRODUCTION

## 1.1 General problematic and context

In the practice of engineering, energy is a fundamental concept where it is common to manage dynamic systems by energy transforming elements. This perspective is very useful to study complex non linear systems, since they can be decomposed in simpler subsystems that can be interconnected between them, where the sum of its components determine the behaviour of the entire system. [1].

Port -based modelling provides an unified framework for the modelling of systems belonging to different physical domains such as mechanical, electrical, hydraulic, thermal, among others [2]. The language that these physical domains share is energy. When two physical systems interacts, there is a flow of energy from a system to another one. The flow of energy determines the dynamic of the system and to control it in a desired way it is necessary to manipulate the interchange of energy [3]. It is appropriate to represent the interactions between two systems by a bilateral relationship, thus the concept of port, defined as an interface in which a system is related with other systems [3].

Port-Hamiltonian (PH) models are widely accepted in the control community due to the principle of modularity and emphasis on physical structure and interconnections. The PH formulation can be used to model complex multi domain physical systems. There are several advantages using a PH approach such as the Hamiltonian can be used directly as the basis to construct a candidate Lyapunov function with the properties of passivity, stability, finite $L_2$ gain, etc.[4]. The theory related with Port-Hamiltonian Systems (PHS) is developed in [5].

In [6] the equations related with the fluid system elements are presented, where a level control of high performance is implemented using the technique of interconnection damping assignment passivity based control (IDA -PBC) for interconnected tanks circuits. The method proposed in [7] can manage several tanks with non linear dynamics, while mass balance physics principles are used. In [8] a control algorithm for a reduced PHS model of the shallow water equations (also called equations of Saint Venant) [9] is presented. In [8] infinitesimal volume and momentum densities are used like state variables, and the sum of kinetic and potential energies as the total Hamiltonian of the system.

Traditionally control design problems have been treated from a signal processing view. The plant to be controlled and the controller are seen as elements that process input signals into output signals. The control objectives are designed to maintain the error signals as small as possible, while the effect of the disturbances is reduced despite the presence of unmodelled dynamics [1]. On the other hand in [10] a framework is presented based on the interpretation of the control as a mathematical model from physics principles.

The action of a controller can be considered like another dynamic system, commonly implemented in a computer, interconnected with the process to modify their performance. The control problem can be proposed as finding a dynamic system able to change the total energy function to a desired form. This technique is known as energy shaping, it is the essence of the passivity based control, and it is very useful in mechanical systems [1].

In [11] the beginnings of the idea of energy shaping is applied to design the control of a manipulator robot, while in [12] these ideas are used to solve classes of Euler-Lagrange systems. In [13] a tutorial of some adaptive control algorithm for manipulators robots is shown where the term PBC is used to define the methodology of controller design, where the objective is to get a passive system with a desired energy stored function.

Two approaches to the selection of the controller can be distinguished. The first is

similar to the classic design based on Lyapunov, where the stored function is selected first, then the controller is chosen to satisfy the objective. In [14] an adaptive controller to minimize the torque ripple in permanent magnet synchronous motors (PMSM) is based on the same principles of “Energy shaping and damping injection". In [15, 16, 17, 18] more applications of controllers based on these same principles can be found. The second approach is related to energy balance of mechanical systems. The energy stored function in closed loop is obtained as the result of the selection of the interconnection of subsystems and the damping. In [19] is the first time that the idea of the analysis of stability is shown. The extension to the design of a controller was presented in [20] and [21]. From these works some applications were obtained: mass balance systems [22],electrical machines [23], power systems [24], magnetic levitation and power converters [25]. The examples described denote the diversity of applications where IDA-PBC control can be implemented.

In [26] new results on rejection of unmatched external disturbances on PHS using Control by interconnection (CBI) is presented. The disturbance rejection problem was addressed adding integral action and there was no need of change of coordinates, keeping the original state vector and being a simpler formulation. The methods presented were applied in two examples: an LC network and a speed control PMSM.

A PBC design for stabilization of a DC-DC buck converter subject to non linear load and matched or unmatched disturbances is presented in [27]. To ensure stability and robustness in closed loop the controller was designed within the PHS framework, also integral action was added to reject constant disturbances. The matching equation was solved by construction i.e. there was no need for solving partial differential equations(PDEs).

In [28] an heterogeneous bidirectional string of vehicles can be modelled as PHS, a non lineal local distributed control with integral actions was used, the proposed control

actions consist into modelling the distance between the vehicles as virtual springs and dampers where the control forces consists of spring forces.

Open channel flows are surfaces directly exposed to the atmosphere pressure. Examples of open channel flows are rivers, estuaries, and artificial structures: irrigation, drainage channels and sewers. Researchers and engineers have being studying rivers for many years. Rivers phenomena e.g. floods can cause a great effect in the human activities. Civil engineering is interested in the study of hydraulic structures to control the natural river behaviour. Flood control and water supply are important aspects that can improve the life quality of many people. Hydroelectric power plants that are located in regulated rivers require an accurate level control. Regulated rivers used to carry water to consumers that need to ensure enough water quantity upstream. A desired water level is reached by the utilization of gates combined with sewer systems [29].

The design of an automatic control to regulate river levels needs accurate models. Saint Venant equations are one of the most popular models used by hydraulic engineers to express the behavior of open channel flows. Saint Venant equations are nonlinear partial differential equations that represent the mass and momentum conservation for one-dimensional open channel flow. Saint Venant equations are difficult to analyze and simulate.

Normally three relevant assumptions are made to study the water phenomena in hydraulic structures: the fluid is homogeneous and incompressible, the flow is steady and the pressure distribution is hydrostatic.

Some recent works managed the problem of controlling the water level from different approaches. From classical control techniques such as [30], where a proportional integrative derivative (PID) controller is applied to get a high precision water tank level using a programmable logic controller (PLC) in a cascade control scheme. In [31] a mathematical

model of a water tank is developed and probed in a real tank. The system is controlled by an adaptive control with recursive identification, to reach a desired tank level manipulating the flow rate entry through a solenoid valve. In [32] a parametric reduced-order approximation is obtained from an infinite dimensional model and applied in an open-channel flow for hydroelectricity. The open-channel hydraulic system is represented using input delay linear parameter- varying (LPV) models. The model is based in Saint Venant equations. They obtain an accurate approximated model conformed by a rational transfer function plus input time delays. Stochastic Model Predictive Control (MPC) for a regulated irrigation channels is analyzed in [33]. In [34] a distributed model predictive control (DMPC) strategy based on linearized Saint Venant equations is applied in a multi reach open- channel system. A Saint Venant reduced order model to control water level used for hydroelectric production in open channels is developed in [35].

The contribution of this thesis is to find a model based on basic hydraulic elements that represents the dynamics of the micro-channel. The assumptions for modelling the micro-channel as a group of tanks + pipes are that the tanks represent the potential energy accumulation, whilst the pipes represent the kinetic energy component, and the channel can be represented by the sum of potential and kinetic energy. The advantage of the model proposed here is to have a similar model to [8] (where the authors reduced an infinite dimensional model to get a port controlled Hamiltonian finite dimensional system equivalent to the Saint Venant equations) with a simplified approach, using ideas shown in [7] (circuit of tanks interconnected), but adding a pipe that stores kinetic energy, being a combination of $\mathrm{N}$ tanks and pipes models. The total energy equation in [8] considers the slope, while in this work the slope is part of the input vector related with a pressure difference, giving us the possibility to manage the slope like an input, separating it from the total energy equation.

The control law is based on energy shaping principles within a PHS framework. A pool

is defined as the space divided by two consecutive sluice gates. This space is modelled as a group of interconnected tanks and pipes. The control is based on this interconnection, where the control variable is the level in a specific tank in a pool, with the manipulation of the resistance (equivalent to the gate position) at the final pipe.

**Figure** 1.1: Micro-channel.

The model found here and the control algorithm designed will be implemented in an experimental micro channel located at the systems control laboratory in Universidad de Concepción, see Figure 1.1. The micro channel has a flow sensor, ultrasonic level sensors, a water pump, and actuators (sluice gates) that allow water pass between pools. The simulations take into account the parameters of the micro channel to compare the results of the simulations with the experimental plant.

## 1.2 Objectives

### 1.2.1 General Objective

To establish the model of the micro channel within the PHS framework together with a control law that allows to obtain a desired level, and implement the designed control on the real plant.

### 1.2.2 Specific Objectives

- To formulate an hydraulic inspired interconnected PHS model for the micro-channel setup.
- To experimentally identify the basic elements of the interconnected PHS model.
- To propose and test a controller design based on the total hydraulic-mechanical energy as a local Lyapunov function.
- To propose and test a controller design that includes integral action to reject constant disturbances and possible modelling errors.

## 1.3 Thesis scope and limitations

The scope of this thesis is to implement a control law based on the total hydraulic-mechanical energy as a local Lyapunov function and an integral action controller (IAC) to get a desired level in a determined micro-channel section using MATLAB® - Simulink® .

To connect the MATLAB® - Simulink® model with the micro-channel PLC. To observe the performance of the simulated and the implemented controllers.

The limitation of this thesis is the number of instruments that can be used to determine the number of the subsystems that can be interconnected.

## 1.4 Organization of the thesis and Methodology

- In Chapter 2 Preliminaries and PHS micro-channel model development. The existing bibliography related to PHS, modelling and design techniques of controllers based in energy shaping is reviewed. The equations of potential and kinetic energy, finding the state variables in a PHS framework are presented. The micro-channel PHS model is shown.
- In Chapter 3 The model identification method is shown using ordinary least squares (OLS) based on a basic element identification.
- In Chapter 4 A controller was designed using the total hydraulic-mechanical energy as a local Lyapunov function. The controller is simulated and implemented in the micro-channel experimental plant.
- In Chapter 5 An integral action controller is deduced from a CbI interpretation. The IAC is simulated and implemented in the micro-channel experimental plant.
- In Chapter 6 General conclusions are presented.

## 1.5 Publications

### 1.5.1 Publications related to the topic of this thesis

- N. Cisneros, H. Ramírez, and A. J. Rojas, “Port Hamiltonian modelling and control of a micro-channel,” in 2019 Australian New Zealand Control Conference (ANZCC), Nov 2019, pp. 82–87.
- Nelson E. Cisneros, Alejandro J. Rojas , and Héctor Ramírez,"Port Hamiltonian system model identification of a micro-channel". in 21st IFAC World Congress in Berlin, 2020, Accepted.
- Nelson E. Cisneros, Alejandro J. Rojas , and Héctor Ramírez,"Port Hamiltonian modelling and control of a micro-channel experimental plant", submitted to IEEE Access, 2020.

### 1.5.2 Other publications

- R. M. Alarcón, O. A. Briones, N. E. Cisneros, M. A. Suárez and A. J. Rojas, "Micro-velocimeter for an open channel flow: a simple and economical alternative," 2019 IEEE CHILEAN Conference on Electrical, Electronics Engineering, Information and Communication Technologies (CHILECON), Valparaiso, Chile, 2019, pp. 1-6.

# 2. MODEL FORMULATION AND EXPERIMENTAL SETUP

## 2.1 Introduction

Cyclo passive systems are defined by the existence of a storage function (nonnegative in case of passivity) satisfying the dissipation inequality with respect to the supply rate $s(u, y) = u^\top y$. Port-Hamiltonian systems (PHS) are endowed with the property of cyclo-passivity as a consequence of their system formulation [5]. In fact, PHS arise from first principles physical modelling. They are defined in terms of a Hamiltonian function together with two geometric structures (corresponding, respectively, to the power-conserving interconnection and energy dissipation), which are such that the Hamiltonian function automatically satisfies the dissipation inequality.

### 2.1.1 PHS formulation

An input-state-output PHS with input and output spaces $U = Y = \mathbb{R}^m$, is given as[5].

$$\begin{aligned} \dot{x} &= [J(x) - R(x)]\frac{\partial H}{\partial x}(x) + g(x)u \\ y &= g^\top(x)\frac{\partial H}{\partial x}(x) \end{aligned} \tag{2.1}$$

Where the $n$ x $n$ matrices $J(x)$, $R(x)$ satisfy $J(x) = -J^{\top}(x)$ and $R(x) = R^{\top}(x) \geq 0$. According to the properties of $J(x)$, $R(x)$, it immediately follows that [5].

$$\frac{dH}{dt}(x(t)) = \frac{\partial^{\top} H}{\partial x}(x(t))\dot{x}(t) \tag{2.2}$$

In this work a model of a micro-channel represented by a series of tanks and pipes connected in cascade using physical variables like pressure and flow is obtained. The reason to use a physical model based on the interchange of energy is to maintain a precise and simple model of the micro-channel.

## 2.2 Fluid Equations

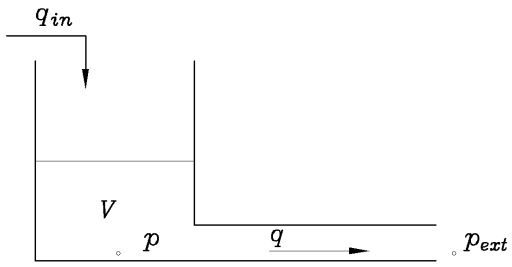


**Figure** 2.1: Tank + pipe schema

In this section the equations related with the dynamics of the fluid in a tank and pipe are shown.

### 2.2.1 Basic definitions

The next equations are obtained according to [6]. The volume $(m^3)$ contained in a tank is described by $V = \mathrm{A}h$, where $\mathrm{A}$ is the cross sectional area $(m^2)$ and $h$ is the water level height $(m)$. The equation for the pressure $p$ $(N/m^2)$ is $p \approx \rho g h$, where $\rho$ is the water density $(Kg/m^3)$ and $g$ is the gravity $(m/s^2)$, it is approximately equal to the product of density, the gravity and the height of the fluid. The variation of the volume in the tank is equal to the difference between the inlet flow and the outlet flow:

$$\frac{dV}{dt} = q_{in} - q_1 \tag{2.3}$$

The momentum $\Pi$ $(Ns/m^2)$ is equal to the product of the fluid inertance $\mathrm{I}$ $(Ns^2/m^5)$ with the flow $q$ $(m^3/s)$, the expression is: $\Pi = \mathrm{I}q$. The fluid capacitance of a tank $\mathrm{C_f}$ $(m^5/N)$ is: $\mathrm{C_f} = \frac{\mathrm{A}}{\rho g}$. The integral of the pressure difference $(N/m^2)$ is defined to be the momentum, this is equivalent to

$$\frac{d\Pi}{dt} = \mathrm{I}\frac{d(q)}{dt} = p_1 - p_{ext} \tag{2.4}$$

The presence of the gate can be represented by a fluid resistance $u$ $(Ns/m^5)$ that is equal to the relation between the difference of pressure and the flow $u = \frac{\Delta p}{q}$.

## 2.3 The total energy equation

An expression of the volume as function of the pressure and the capacitance of the fluid is obtained as: $V = \frac{\mathrm{A}}{\rho \mathrm{g}} p = \mathrm{C_f} p$. According to the definition of the stored energy in an ideal fluid capacitor the potential energy $(J)$ is: $\frac{\mathrm{C_f}}{2} p^2 = \frac{1}{2} \frac{V^2}{\mathrm{C_f}}$

The stored energy $(J)$ in an ideal fluid inertance is: $\frac{1}{2} \mathrm{I} q^2 = \frac{1}{2} \frac{\Pi^2}{\mathrm{I}}$ The partial derivative of the kinetic energy regarding the momentum is $\frac{\Pi}{\mathrm{I}} = q$. Finally, the total energy $(J)$ is $\frac{1}{2} \frac{V^2}{\mathrm{C_f}} + \frac{1}{2} \frac{\Pi^2}{\mathrm{I}}$

## 2.4 One subsystem PHS model

In this section the PHS model of one subsystem is shown. Each subsystem is the interconnection of one tank and one pipe between them. The pressure fluid momentum is equal to the difference between the pressure inside the tank and the downstream pressure.

$$\dot{\Pi}_1 = p_1 - p_{ext} \tag{2.5}$$

The volume variation is equal to the input and output flow difference.

$$\dot{V} = q_{in} - q_1 \tag{2.6}$$

The PHS is formulated considering (2.5) and (2.6).

$$\begin{bmatrix} \dot{V} \\ \dot{\Pi} \end{bmatrix} = \underbrace{\begin{bmatrix} 0 & -1 \\ 1 & 0 \end{bmatrix}}_{J(x)-R(x)} \underbrace{\begin{bmatrix} p_1 \\ q_{ext} \end{bmatrix}}_{\frac{\partial H}{\partial x}} + \underbrace{\begin{bmatrix} 1 & 0 \\ 0 & -1 \end{bmatrix}}_{g(x)} \underbrace{\begin{bmatrix} q_{in} \\ p_{ext} \end{bmatrix}}_{d(x)} \tag{2.7}$$

$$g^{\top}(x) = \begin{bmatrix} 1 & 0 \\ 0 & -1 \end{bmatrix} \tag{2.8}$$

$$\frac{\partial H}{\partial x} = \begin{bmatrix} p_1 \\ q_1 \end{bmatrix} \tag{2.9}$$

$$y = \underbrace{\begin{bmatrix} 1 & 0 \\ 0 & -1 \end{bmatrix}}_{g^{\top}(x)} \underbrace{\begin{bmatrix} p_1 \\ q_1 \end{bmatrix}}_{d(x)} = \begin{bmatrix} p_1 \\ -q_1 \end{bmatrix} \tag{2.10}$$

The equations above are the PHS model of a tank and a pipe. The intensive variables are the pressure inside the tank and the output flow. The extensive variables are the volume and the pressure momentum derivatives. The input flow and the external pressure compose the system disturbance map. The pressure inside the tank and the output flow with negative sign are part of the output vector.

## 2.5 PHS model of a finite number of interconnected subsystems

We present the PHS model of the interconnection of two subsystems and the general form for a finite number of subsystems.

### 2.5.1 Interconnection of two subsystems

The model of two subsystems interconnected between them is presented. The next conditions show the interconnections between two subsystems.

$$u_2 = y_1$$

$$u_1 = -y_2$$

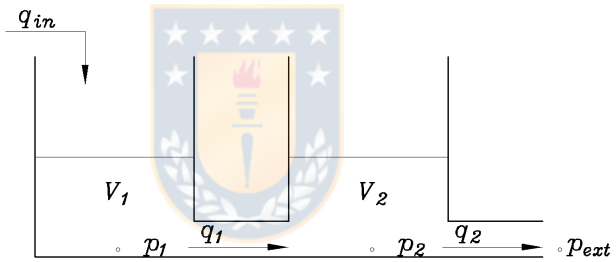


**Figure** 2.2: Interconnection of two tanks and pipes

The next equations represent the model of the interconnection of two subsystems.

$$\dot{V}_1 = q_{in} - q_1 \tag{2.11}$$

$$\dot{\Pi}_1 = p_1 - p_2 \tag{2.12}$$

$$\dot{V}_2 = q_1 - q_2 \tag{2.13}$$

$$\dot{\Pi}_2 = p_2 - p_{ext} \tag{2.14}$$

The PHS model is:

$$\begin{bmatrix} \dot{V}_1 \\ \dot{\Pi}_1 \\ \dot{V}_2 \\ \dot{\Pi}_2 \end{bmatrix} = \underbrace{\begin{bmatrix} 0 & -1 & 0 & 0 \\ 1 & 0 & -1 & 0 \\ 0 & 1 & 0 & -1 \\ 0 & 0 & 1 & 0 \end{bmatrix}}_{J(x)-R(x)} \underbrace{\begin{bmatrix} p_1 \\ q_1 \\ p_2 \\ q_2 \end{bmatrix}}_{\frac{\partial H}{\partial x}} + \underbrace{\begin{bmatrix} 1 & 0 \\ 0 & 0 \\ 0 & 0 \\ 0 & -1 \end{bmatrix}}_{g(x)} \underbrace{\begin{bmatrix} q_{in} \\ p_{ext} \end{bmatrix}}_{d(x)} \tag{2.15}$$

$$y = \underbrace{\begin{bmatrix} 1 & 0 & 0 & 0 \\ 0 & 0 & 0 & -1 \end{bmatrix}}_{g^\top(x)} \underbrace{\begin{bmatrix} p_1 \\ q_1 \\ p_2 \\ q_2 \end{bmatrix}}_{\frac{\partial H}{\partial x}} = \begin{bmatrix} p_1 \\ -q_2 \end{bmatrix} \tag{2.16}$$

The pressure and momentum variables of two subsystems are shown in (2.15) while equation (2.16) represents the system output. The output flow and the downstream pressure of the first subsystem interconnects both subsystems. The first subsystem pressure and the last output flow with negative sign are part of the output vector.

### 2.5.2 General model representation

The next equations generalize the model for N number subsystems.

$$\begin{bmatrix} \dot{V}_1 \\ \dot{\Pi}_1 \\ \vdots \\ \dot{V}_{\mathrm{N}} \\ \dot{\Pi}_{\mathrm{N}} \end{bmatrix} = \begin{bmatrix} 0 & -1 & \cdots & 0 & 0 \\ 1 & 0 & \cdots & 0 & 0 \\ \vdots & \vdots & \ddots & \vdots & \vdots \\ 0 & 0 & \cdots & 0 & -1 \\ 0 & 0 & \cdots & 1 & 0 \end{bmatrix} \begin{bmatrix} p_1 \\ q_1 \\ \vdots \\ p_{\mathrm{N}} \\ q_{\mathrm{N}} \end{bmatrix} + \begin{bmatrix} 1 & 0 \\ 0 & 0 \\ \vdots & \vdots \\ 0 & 0 \\ 0 & -1 \end{bmatrix} \begin{bmatrix} q_{in} \\ \vdots \\ p_{ext} \end{bmatrix} \tag{2.17}$$

$$y = \begin{bmatrix} 1 & 0 & \cdots & 0 & 0 \\ 0 & 0 & \cdots & 0 & -1 \end{bmatrix} \begin{bmatrix} p_1 \\ q_1 \\ \vdots \\ p_{\mathrm{N}} \\ q_{\mathrm{N}} \end{bmatrix} = \begin{bmatrix} p_1 \\ -q_{\mathrm{N}} \end{bmatrix} \tag{2.18}$$

$\mathrm{N} \in \mathbb{N}$ in (2.17) and (2.18) represents the finite number of subsystems interconnected in series between them. The output vector is still composed of the first subsystem pressure and the last output flow with negative sign being independent of the subsystems interconnection number.

## 2.6 PHS model with slope

In this section the micro-channel slope is considered as a model disturbance. The PHS model of two subsystems with slope is shown to observe its effect, then the general model with slope is presented.

### 2.6.1 Two subsytems PHS model with slope

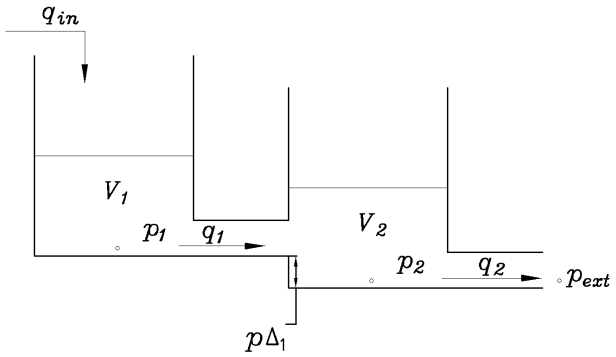


**Figure** 2.3: Interconnection of two subsystems considering the micro-channel slope.

The micro-channel slope is considered like a pressure drop. In the next equations the pressure drop caused by the micro-channel slope is included in the model of two subsystems, see (2.15).

The equation (2.4) is modified due to the slope.

$$\dot{V}_1 = q_{in} - q_1 \tag{2.19}$$

$$\dot{\Pi}_1 = p_1 - (p_2 - p_{\Delta 1}) \tag{2.20}$$

$$\dot{V}_2 = q_1 - q_2 \tag{2.21}$$

$$\dot{\Pi}_2 = p_2 - p_{ext} \tag{2.22}$$

The PHS model is:

$$\begin{bmatrix} \dot{V}_1 \\ \dot{\Pi}_1 \\ \dot{V}_2 \\ \dot{\Pi}_2 \end{bmatrix} = \underbrace{\begin{bmatrix} 0 & -1 & 0 & 0 \\ 1 & 0 & -1 & 0 \\ 0 & 1 & 0 & -1 \\ 0 & 0 & 1 & 0 \end{bmatrix}}_{J(x)-R(x)} \underbrace{\begin{bmatrix} p_1 \\ q_1 \\ p_2 \\ q_2 \end{bmatrix}}_{\frac{\partial H}{\partial x}} + \underbrace{\begin{bmatrix} 1 & 0 & 0 \\ 0 & 1 & 0 \\ 0 & 0 & 0 \\ 0 & 0 & -1 \end{bmatrix}}_{g(x)} \underbrace{\begin{bmatrix} q_1 \\ p_{\Delta 1} \\ p_{ext} \end{bmatrix}}_{d(x)} \tag{2.23}$$

Thus the system output is:

$$y = \underbrace{\begin{bmatrix} 1 & 0 & 0 & 0 \\ 0 & 1 & 0 & 0 \\ 0 & 0 & 0 & -1 \end{bmatrix}}_{g^\top(x)} \underbrace{\begin{bmatrix} p_1 \\ q_1 \\ p_2 \\ q_2 \end{bmatrix}}_{\frac{\partial H}{\partial x}} = \begin{bmatrix} p_1 \\ q_1 \\ -q_2 \end{bmatrix} \tag{2.24}$$

The cost of the inclusion of the pressure drop representing the slope of the micro-channel in the input map is the appearance of an intermediate flow $q_1$ in the port conjugated variables (outputs).

### 2.6.2 PHS model general form with slope

The next equations show the model of $\mathrm{N} \in \mathbb{N}$ number of subsystems with slope.

$$\begin{bmatrix} \dot{V}_1 \\ \dot{\Pi}_1 \\ \vdots \\ \dot{V}_{\mathrm{N}} \\ \dot{\Pi}_{\mathrm{N}} \end{bmatrix} = \begin{bmatrix} 0 & -1 & \cdots & 0 & 0 \\ 1 & 0 & \cdots & 0 & 0 \\ \vdots & \vdots & \ddots & \vdots & \vdots \\ 0 & 0 & \cdots & 0 & -1 \\ 0 & 0 & \cdots & 1 & 0 \end{bmatrix} \begin{bmatrix} p_1 \\ q_1 \\ \vdots \\ p_{\mathrm{N}} \\ q_{\mathrm{N}} \end{bmatrix} + \begin{bmatrix} 1 & 0 & \cdots & 0 & 0 \\ 0 & 1 & \cdots & 0 & 0 \\ \vdots & \vdots & \ddots & \vdots & \vdots \\ 0 & 0 & \cdots & 0 & 0 \\ 0 & 0 & \cdots & 0 & -1 \end{bmatrix} \begin{bmatrix} q_{in} \\ p_{\Delta 1} \\ \vdots \\ 0 \\ p_{ext} \end{bmatrix} \tag{2.25}$$

$$y = \begin{bmatrix} 1 & 0 & \cdots & 0 & 0 \\ 0 & 1 & \cdots & 0 & 0 \\ \vdots & \vdots & \ddots & \vdots & \vdots \\ 0 & 0 & \cdots & 0 & 0 \\ 0 & 0 & \cdots & 0 & -1 \end{bmatrix} \begin{bmatrix} p_1 \\ q_1 \\ \vdots \\ p_{\mathrm{N}} \\ q_{\mathrm{N}} \end{bmatrix} = \begin{bmatrix} p_1 \\ q_1 \\ \vdots \\ 0 \\ -q_{\mathrm{N}} \end{bmatrix} \tag{2.26}$$

The output vector is composed of the pressure in the first subsystem, the output flow of the last subsystem and the intermediate flows caused by the slope inclusion in the disturbance vector.

## 2.7 The actuator as a controllable fluid resistance

The actuator is included as a controllable fluid resistance. Firstly the actuator is included in one subsystem. Then, two subsystems with an uncontrollable fluid resistance and a controllable fluid resistance are presented. Finally the general model is shown.

### 2.7.1 Analysis of one subsystem

To introduce the actuator the case of one subsystem and one actuator is analyzed.

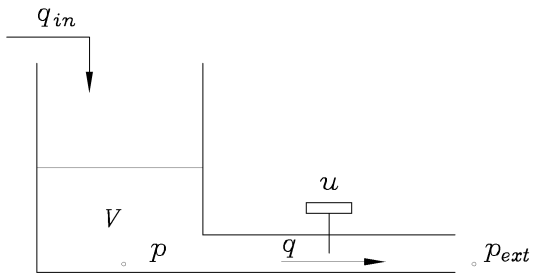


**Figure** 2.4: One tank and pipe with a gate

The actuator is represented by a controllable fluid resistance being the input control signal $u$. $u$ is in series with an inertance $\mathrm{I}_1$. (2.20) is modified to introduce the presence of the controllable fluid resistance. The next equations describe the behavior of the micro-channel with the controllable fluid resistance inclusion.

$$\mathrm{I}_1 \frac{d(q_1)}{dt} + uq_1 = p_1 - p_2 \tag{2.27}$$

$$\dot{\Pi}_1 = \mathrm{I}_1 \frac{d(q_1)}{dt}$$

$$\dot{\Pi}_1 = p_1 - p_2 - uq_1 \tag{2.28}$$

The model (2.7) changes to:

$$\begin{bmatrix} \dot{V}_1 \\ \dot{\Pi}_1 \end{bmatrix} = \underbrace{\begin{bmatrix} 0 & -1 \\ 1 & -u \end{bmatrix}}_{J(x)-R(x)} \underbrace{\begin{bmatrix} p_1 \\ q_1 \end{bmatrix}}_{\frac{\partial H}{\partial x}} + \underbrace{\begin{bmatrix} 1 & 0 \\ 0 & -1 \end{bmatrix}}_{g(x)} \underbrace{\begin{bmatrix} q_{in} \\ p_{ext} \end{bmatrix}}_{d(x)} \tag{2.29}$$

$$y = \underbrace{\begin{bmatrix} 1 & 0 \\ 0 & -1 \end{bmatrix}}_{g^T(x)} \underbrace{\begin{bmatrix} p_1 \\ q_1 \end{bmatrix}}_{\frac{\partial H}{\partial x}} = \begin{bmatrix} p_1 \\ -q_1 \end{bmatrix} \tag{2.30}$$

### 2.7.2 Analysis of two subsystems

The PHS micro-channel model includes the fluid resistances. An uncontrollable fluid resistance $\mathrm{R_{f1}}$ and a controllable fluid resistance $u$ are considered, being $u$ the input control signal.

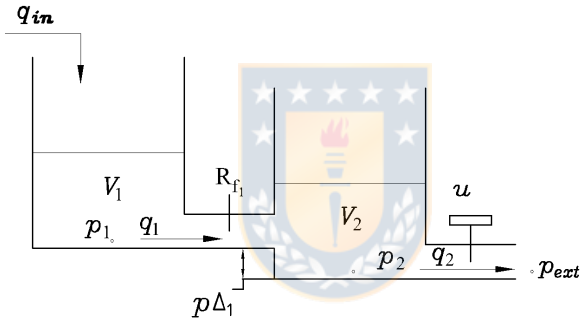


**Figure** 2.5: Interconnection of two tanks and pipes considering a slope and gates in the output

The new equations are:

$$\dot{V}_1 = q_{in} - q_1 \tag{2.31}$$

$$\dot{\Pi}_1 = p_1 - (p_2 - p_{\Delta 1}) - \mathrm{R_{f1}} q_1 \tag{2.32}$$

$$\dot{V}_2 = q_1 - q_2 \tag{2.33}$$

$$\dot{\Pi}_2 = p_2 - p_{ext} - u q_2 \tag{2.34}$$

The PHS model is:

$$\begin{bmatrix} \dot{V}_1 \\ \dot{\Pi}_1 \\ \dot{V}_2 \\ \dot{\Pi}_2 \end{bmatrix} = \underbrace{\begin{bmatrix} 0 & -1 & 0 & 0 \\ 1 & -\mathrm{R_{f1}} & -1 & 0 \\ 0 & 1 & 0 & -1 \\ 0 & 0 & 1 & -u \end{bmatrix}}_{J(x)-R(x)} \underbrace{\begin{bmatrix} p_1 \\ q_1 \\ p_2 \\ q_2 \end{bmatrix}}_{\frac{\partial H}{\partial x}} + \underbrace{\begin{bmatrix} 1 & 0 & 0 \\ 0 & 1 & 0 \\ 0 & 0 & 0 \\ 0 & 0 & -1 \end{bmatrix}}_{g(x)} \underbrace{\begin{bmatrix} q_{in} \\ p_{\Delta 1} \\ p_{ext} \end{bmatrix}}_{d(x)} \tag{2.35}$$

Thus the output of the system is:

$$y = \underbrace{\begin{bmatrix} 1 & 0 & 0 & 0 \\ 0 & 1 & 0 & 0 \\ 0 & 0 & 0 & -1 \end{bmatrix}}_{g^T(x)} \underbrace{\begin{bmatrix} p_1 \\ q_1 \\ p_2 \\ q_2 \end{bmatrix}}_{\frac{\partial H}{\partial x}} = \begin{bmatrix} p_1 \\ q_1 \\ -q_2 \end{bmatrix} \tag{2.36}$$

### 2.7.3 General model considering a slope and a controllable fluid resistance to represent the actuator

This section shows the general micro-channel model that includes its dynamics such as the volume and the fluid pressure momentum variations, the micro-channel slope and the actuator represented by a controllable fluid resistance of $\mathrm{N}$ number of subsystems.

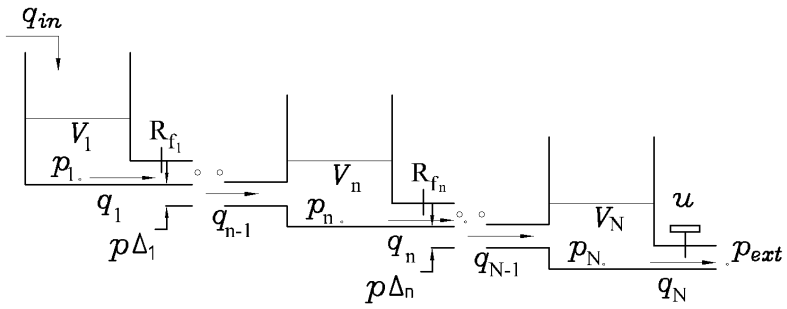


**Figure** 2.6: Interconnection of N tanks and pipes considering a slope and a gate in the output.

The next model considers $\mathrm{N} \in \mathbb{N}$ number of tanks and pipes with slope, see Figure 2.6. All the subsystems have uncontrollable fluid resistances except in the last subsystem where a controllable fluid resistance $u$ is placed on the interconnection matrix diagonal.

$$\begin{bmatrix} \dot{V}_1 \\ \dot{\Pi}_1 \\ \vdots \\ \dot{V}_\mathrm{N} \\ \dot{\Pi}_\mathrm{N} \end{bmatrix} = \begin{bmatrix} 0 & -1 & \cdots & 0 & 0 \\ 1 & -\mathrm{R_{f1}} & \cdots & 0 & 0 \\ \vdots & \vdots & \ddots & \vdots & \vdots \\ 0 & 0 & \cdots & 0 & -1 \\ 0 & 0 & \cdots & 1 & -u \end{bmatrix} \begin{bmatrix} p_1 \\ q_1 \\ \vdots \\ p_\mathrm{N} \\ q_\mathrm{N} \end{bmatrix} + \begin{bmatrix} 1 & 0 & \cdots & 0 \\ 0 & 1 & \cdots & 0 \\ \vdots & \vdots & \ddots & \vdots \\ 0 & 0 & \cdots & 0 \\ 0 & 0 & \cdots & -1 \end{bmatrix} \begin{bmatrix} q_{in} \\ p_{\Delta 1} \\ \vdots \\ p_{ext} \end{bmatrix} \tag{2.37}$$

$$y = \begin{bmatrix} 1 & 0 & \cdots & 0 \\ 0 & 1 & \cdots & 0 \\ \vdots & \vdots & \ddots & \vdots \\ 0 & 0 & \cdots & 0 \\ 0 & 0 & \cdots & -1 \end{bmatrix} \begin{bmatrix} p_1 \\ q_1 \\ \vdots \\ p_N \\ q_\mathrm{N} \end{bmatrix} = \begin{bmatrix} p_1 \\ q_1 \\ \vdots \\ -q_\mathrm{N} \end{bmatrix} \tag{2.38}$$

The generalized micro-channel model shows $\mathrm{N}$ tanks and pipes interconnected in series to represent the behavior of the micro-channel. The model presented by [8] starts with the port-based modelling of shallow water flows. Applying a discretization method, a PCH finite-dimensional system is obtained. On the other hand in this thesis we start with a concentrated-parameter model, interconnecting basic elements equivalent to capacitors and inductance to obtain the total energy equation. Comparing the resultant model with the model obtained from the Saint Venant equations reduction in [8], we can highlight the convergence of both models with light differences. The model presented here considers the micro-channel slope as part of the disturbance vector whilst in [8] the slope is included in the total energy equation. We consider two types of resistance, being the controllable resistance the sluice gate representation. The model presented in [8] includes the Manning-Strickler formula as the dissipative term.

## 2.8 Micro-channel experimental plant

**Figure** 2.7: Experimental setup micro-channel.

The micro-channel is an experimental plant that can represent open channel flow hydraulic phenomena at scale, Figure 2.7. The micro-channel has installed the instruments detailed in Table 2.1. The software used is RSlogix® , MATLAB® and Simulink® .

**Table** 2.1: Micro-channel instrumentation and control

| Number | Instrument | Brand |
|---|---|---|
| 2 | Ultrasonic level sensors | Endress+Hauser® Prosonic M |
| 1 | Ultrasonic level sensors | Maxbotix ® |
| 1 | Ultrasonic level transmitter | Rosemount® |
| 1 | Electromagnetic flow meter | Endress+Houser® Promag 10 |
| 1 | micro sensor of velocity (MSV) | developed in [36] |
| 1 | Linear actuator | Exlar® GSX series |
| 1 | Variable frequency drive (VFD) | Rockwell PowerFlex® |
| 1 | Pneumatic gate | Fisher® Fieldvue® Instruments |
| 1 | PLC | Rockwell Contrologix® |

The micro-channel piping and instrumentation diagram is shown in Figure 2.8.

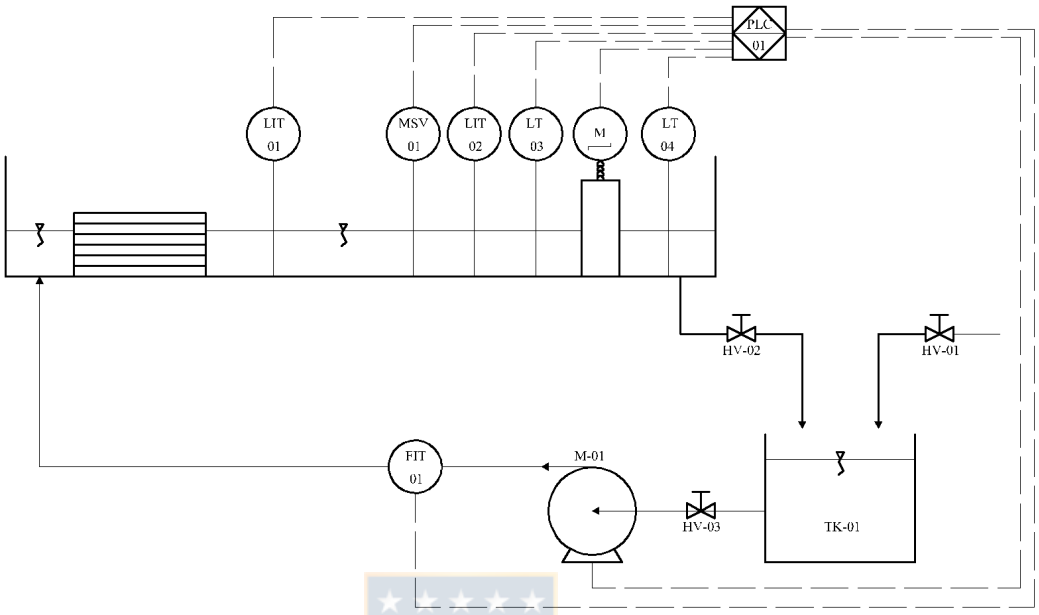


**Figure** 2.8: Piping and instrumentation diagram

Where M-01 is the centrifugal pump that boost the water into the micro-channel. The level sensors are LIT-01, LIT-02, LT-03 and LT-04. The flow sensor FIT-01 is located in the centrifugal pump output. The speed velocimeter MSV-01 is located in the middle of the micro-channel section between the subsystems. All the signals are connected to the PLC-01. Table 2.2 shows the micro-channel dimensions and its slope.

**Table** 2.2: Micro-channel characteristics

| Characteristic | Measure |
|---|---|
| Length | $7[m]$ |
| Width | $0.145[m]$ |
| Height | $0.345[m]$ |
| Slope | $0.328°$ |

## 2.9 Summary

In this chapter the micro-channel PHS model was presented based on the interconnection of basic elements divided in subsystems. The total energy equation is represented by the sum of the potential and the kinetic energy. The potential energy is related with the stored volume in a tank. The kinetic energy describes the water flow through a pipe connected with a tank.

Each subsystem has electrical equivalent elements such as fluid capacitors (capacitors), inertances (inductance) and fluid resistance (resistors). The fluid resistances can be uncontrollable caused by the wall friction and the controllable fluid resistance that is the representation of the actuator (sluice gate). The fluid resistances are located over the pipes and cause pressure drops. The PHS model interconnects several subsystems and considers the slope presented in the micro-channel. The slope can be considered as a pressure drop. The slope can be the same for all the micro-channel or vary in an specific segment depending of the experimental plant. In this thesis the slope was considered as constant in the model.

The micro-channel is an experimental plant used to simulate hydraulic phenomena at scale. The micro-channel experimental plant has level, flow and speed sensors. All the signals are connected to a PLC.

# 3. MODEL IDENTIFICATION

## 3.1 Introduction

The authors of [37] deduced a vocal folds model based on a vocal fluid-structure interaction compared with a mechanical structure equivalent to a mass-spring-damper system. In [38] a micro-channel model is developed based on the interconnection of basic elements also modeled as capacitors, inductance and resistors that represents tanks, pipes and gates respectively. The interconnection of several subsystems (tank-pipe-fluid resistance) generate a good approximation to the behavior of a micro-channel. In [38] the micro-channel fluid capacitance $\mathrm{C_f}$ (equivalent to the electrical capacitance) was found from the geometric structure of the micro-channel. The inertance $\mathrm{I}$ (equivalent to the inductance in an electrical circuit) is more difficult to find because physically there is no pipe . The uncontrollable resistance $\mathrm{R_f}$ related with the friction of the the walls is also difficult to obtain. Finally, the controllable resistance $u$ can be deduced from the sluice gate model. In order to get an accurate model that represents the dynamics of a micro-channel experimental plant, a process of identification has to be done to obtain the model parameters that are difficult to measure.

Recent works apply identification methodologies to different applications such as, [39] where a modified recursive least squares algorithm is used on sparse systems (most coefficients of the impulse responses are zero or non-zero). In [40] various linear methods such as state space (SS) model, autoregressive with exogenous terms (ARX) model and nonlinear methods like nonlinear autoregressive exogenous (NARX) model and Hammerstein-Wiener models are applied to a MIMO process. The validation techniques used are Mean

Squared Error (MSE) and Final Prediction Error (FPE). In [41] ARX and autoregressive moving average exogenous (ARMAX) are used to represent a four wheel mobile robot (FWMR). In [42] a state space model identification methodology is presented. A Chirp signal is used to identify a Hammerstein model for a nonlinear process in [43]. Fixed wing lateral dynamics of an Unmanned Aerial Vehicle (UAV) model are identified using least square error estimation technique in [44]. The model of a coupled tank nonlinear Multiple-Input Multiple-Output (MIMO) system is identified in [44].

## 3.2 Basic Element Identification

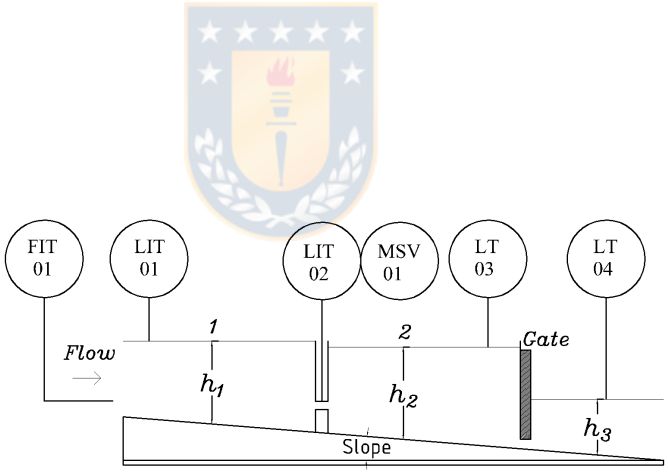


**Figure** 3.1: Schematic representation of two subsystems

To adjust the theoretical PHS structure to the experimental setup, a parameter identification experiment has to be done.

First, we identify two types of interconnected subsystems. The first subsystem considers an uncontrollable resistance. The second subsystem considers a controllable resistance.

Secondly, we validate the model of the subsystems previously identified with the inter-

connection of three subsystems. We interconnect two subsystems with an uncontrollable resistance to one subsystem with a controllable resistance, see 3.3.1. Finally, we design two types of controllers for a model composed of four subsystems, see 3.3.2.

To find the best fitting curve a mathematical procedure called Ordinary Least Squares (OLS) is used, given a set of points.

The experimental setup has four level sensors (LIT-01, LIT-02, LT-03 and LT-04), one flow sensor (FIT-01) and one micro speed velocimeter (MSV-01)[36] that is used to estimate the flow. The flow sensor (FIT-01) registers the input flow directly from the pump output. The micro speed velocimeter (MSV-01) and the level sensor (LIT-02) are located in the middle of the micro-channel section to be identified. The micro-channel section is divided in two subsystems. The first subsystem considers an estimated flow calculated from the speed and level measures as the output flow and it is the input flow for he second subsystem. The identification procedure considers gate position as the control variable. Figure 3.1 indicates the sensors used in the identification experiment. The capacitance is a geometric parameter easy to verify and it is related with the longitudinal section of the micro-channel. The schematic representation of the identified subsystems is shown in Figure 2.5.

### 3.2.1 Subsystem one

The first subsystem considers one tank and one pipe. The output flow is estimated using the speed and the level measures.

$$\frac{\mathrm{I}_1}{\mathrm{T_s}}(q_1(k\mathrm{T_s}+\mathrm{T_s})-q_1(k\mathrm{T_s}))=\frac{\mathrm{A}_1}{\mathrm{C_{f_1}}}h_1(k\mathrm{T_s})-\frac{\mathrm{A}_2}{\mathrm{C_{f_2}}}h_2(k\mathrm{T_s})-\mathrm{R_{f_1}}q_1(k\mathrm{T_s}) \tag{3.1}$$

Reordering:

$$h_1(k\mathrm{T_s}) = \frac{\mathrm{C_{f_1}I_1}}{\mathrm{A_1T_s}}(q_1(k\mathrm{T_s}+\mathrm{T_s}) - q_1(k\mathrm{T_s})) + \frac{\mathrm{C_{f_1}A_2}}{\mathrm{A_1C_{f_2}}}h_2(k\mathrm{T_s}) + \frac{\mathrm{C_{f_1}Rf_1}}{\mathrm{A_1}}q_1(k\mathrm{T_s}) \quad (3.2)$$

From which we have the following parameters:

$$h_1(k\mathrm{T_s}) = \gamma_1(q_1(k\mathrm{T_s}+\mathrm{T_s}) - q_1(k\mathrm{T_s})) + \gamma_2 h_2(k\mathrm{T_s}) + \gamma_3 q_1(k\mathrm{T_s}) \quad (3.3)$$

where $k \in \mathbb{N}$ is the observation number. $\mathrm{T_s}$ is the sample time. $\gamma_1$ and $\gamma_2$ are the model parameters. $h_1$ is the water height level in the first subsystem and $h_2$ is the water height level in the second subsystem. $q_1$ is the output flow of the first subsystem.

### 3.2.2 Subsystem two

In the second subsystem the output flow is estimated from the level measurements before and after the gate. To determine the fluid resistance value we consider the term $\alpha_g = 0.66$ (that is an empirical term), [45]:

$$q_2 = \frac{\mathrm{B}h_3\sqrt{2}}{\sqrt{\left(\frac{h_3^2}{\alpha_g^2 h_g^2} - 1\right)}}\sqrt{g(h_2 - h_3)} \quad (3.4)$$

where $\mathrm{B}$ is the width of the micro-channel $(m)$, $h_2$ is the water level height $(m)$ of the second subsystem, $h_3$ is the water height level after the sluice gate, $g$ is the gravity $(m^2/s)$ and $h_g$ is the sluice gate opening.

Considering the stationary state

$$u = \frac{\Delta P}{q_2} \tag{3.5}$$

$$\frac{\mathrm{I_2}}{\mathrm{T_s}}(q_2(k\mathrm{T_s} + \mathrm{T_s}) - q_2(k\mathrm{T_s})) = \frac{\mathrm{A_2}}{\mathrm{C_{f2}}}h_2(k\mathrm{T_s}) - \mathrm{K_1}h_3(k\mathrm{T_s}) - u(k\mathrm{T_s})q_2(k\mathrm{T_s}) \tag{3.6}$$

The final expression is:

$$\begin{aligned} h_2(k\mathrm{T_s}) = \; & \tfrac{\mathrm{C_{f2}I_2}}{\mathrm{A_2T_s}}(q_2(k\mathrm{T_s} + \mathrm{T_s}) - q_2(k\mathrm{T_s})) + \tfrac{\mathrm{C_{f2}K_1}}{\mathrm{A_2}}h_3(k\mathrm{T_s}) \\ & + \tfrac{\mathrm{C_{f2}}(k\mathrm{T_s})}{\mathrm{A_2}}\rho g(h_2(k\mathrm{T_s}) - h_3(k\mathrm{T_s}))) \end{aligned} \tag{3.7}$$

Replacing with the unknown parameters:

$$\begin{aligned} h_2(k\mathrm{T_s}) = \; & \gamma_4(q_2(k\mathrm{T_s} + \mathrm{T_s}) - q_2(k\mathrm{T_s})) + \gamma_5 h_3(k\mathrm{T_s}) \\ & + \gamma_6 \rho g(h_2(k\mathrm{T_s}) - h_3(k\mathrm{T_s})) \end{aligned} \tag{3.8}$$

where again $k \in \mathbb{N}$ is the time index and $\rho$ is the water density $(Kg/m^3)$. $\gamma_4, \gamma_5$ and $\gamma_6$ are the model parameters.

Table 3.1 resumes the unknown parameters and their definition:

**Table** 3.1: Model parameters to identify.

| Parameter | Definition | Parameter | Definition |
|---|---|---|---|
| $\gamma_1$ | $\frac{C_{f_1} I_1}{A_1 T_s}$ | $\gamma_4$ | $\frac{C_{f_2} I_2}{A_2 T_s}$ |
| $\gamma_2$ | $\frac{C_{f_1} A_2}{A_1 C_{f_2}}$ | $\gamma_5$ | $\frac{C_{f_2} K_1}{A_2}$ |
| $\gamma_3$ | $\frac{C_{f_1} R_{f_1}}{A_1}$ | $\gamma_6$ | $\frac{C_{f_2}}{A_2}$ |

The parameters are estimated using OLS see [46].

### 3.2.3 Two subsystems identification

In this experiment we use (3.3) and (3.8) to identify a subsystem with an uncontrollable resistance interconnected with a subsystem with a controllable resistance. The input flow is $1.5l/s$. A seventh order Pseudo Random Binary Sequence (PRBS) with a period of ten minutes was applied to the gate position, varying between $0.6[cm]$ and $2.6[cm]$ from the channel floor, because these values cause a change in the micro-channel level. The PRBS design parameters such as the period and the order were taken from [47] where an identification process was made to identify the parameters of a similar process. The first half of the experimental data was used to calculate the parameters, whilst the second half of data was used to validate the model. The sample period was $T_s = 0.04s$. Table 3.2 indicates the parameters obtained from the identification method. The area and the capacitance are found directly from the micro-channel geometry ($C_f = \frac{A}{\rho g}$). The identification method gives the inertances, and the uncontrollable fluid resistance caused by the friction of the walls.

**Table** 3.2: Parameters obtained

| Parameter | Value | Parameter | Value |
|---|---|---|---|
| $\gamma_1$ | 11.66 | $A_1$ | 0.1914 |
| $\gamma_2$ | 0.78 | $A_2$ | 0.1914 |
| $\gamma_3$ | 22.52 | $K_1$ | 9.8 |
| $\gamma_4$ | 0.003 | $C_{f1}$ | 0.0195 |
| $\gamma_5$ | 1.0814 | $C_{f2}$ | 0.0195 |
| $\gamma_6$ | 0.9921 | $Rf_1$ | 22.52 |
| | | $I_1$ | 4.6 |
| | | $I_2$ | 0.0294 |

We show the comparison between the experimental data, the identification results and the continuous time data in Figure 3.2 for the height water level of the first subsystem. The figure show a good approximation between the three compared signals.

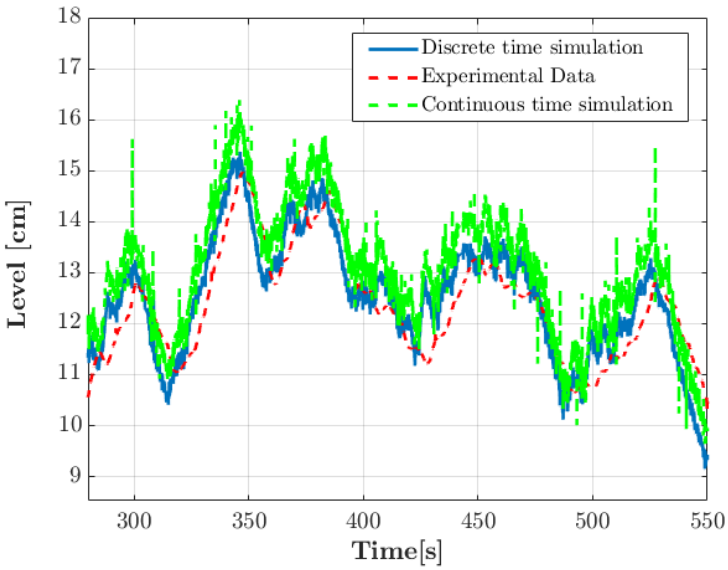


**Figure** 3.2: Model validation first subsystem.

Figure 3.3 shows the results of the simulated , experimental and continuous time simulation height water level for the second subsystem. The compared signals show a similar behavior with the same input signal.

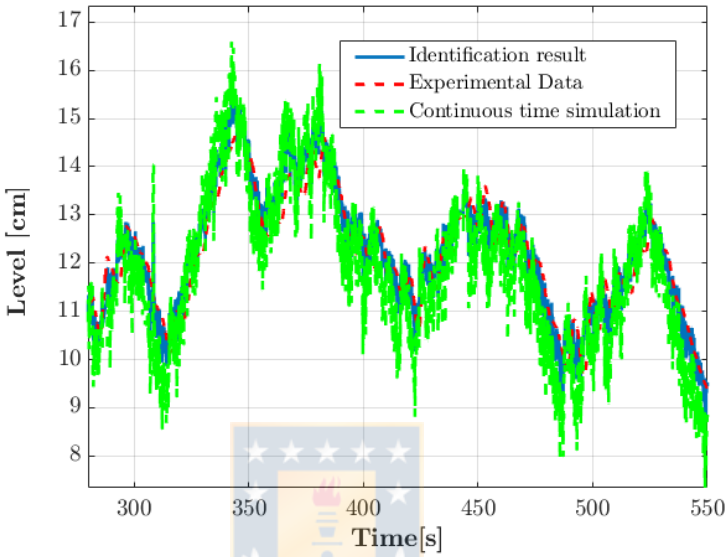


**Figure** 3.3: Model validation second subsystem.

## 3.3 Experimental estimation

### 3.3.1 Three subsystems experiment

An estimation experiment was done using the parameters found previously. Two subsystems (tank, pipe, uncontrollable fluid resistance) and one subsystem (tank, pipe, controllable fluid resistance) interconnected in series were modelled. Each subsystem has a length of $1.32m$. Figure 3.4 shows the model response to changes of different gate positions. The error between the model and the experimental data increases with the level but is acceptable in the operating zone (less than twenty centimeters).

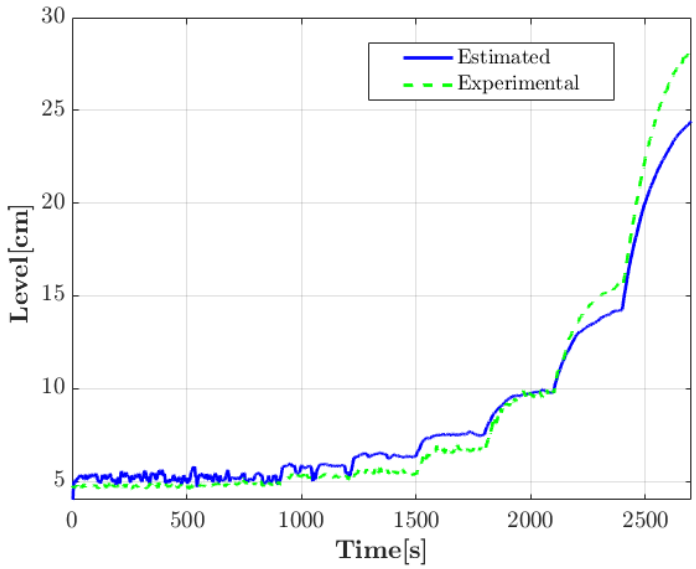


**Figure** 3.4: Model estimation, $h_1$

### 3.3.2 Fluid resistance adjustment

In order to improve the estimation results of the model and the experimental plant the fluid resistance was adjusted. The desired fluid resistance was compared with the fluid resistance calculated from the gate position. The method used to adjust the fluid resistance values was OLS, the structure of the equation is a seventh order polynomial.

$$\hat{u} = \eta_8(u)^7 + \eta_7(u)^6 + \eta_6(u)^5 + \eta_5(u)^4 + \eta_4(u)^3 + \eta_3(u)^2 + \eta_2(u) + \eta_1 \tag{3.9}$$

where $u$ is equal to the difference between the pressure before and after the gate divided by the output flow calculated with (3.4). $\hat{u}$ is the necessary fluid resistance to fit the experimental level with the simulated level. $\hat{u}$ is obtained from simulation. $\eta_n$ are the parameters that adjust $u$ with $\hat{u}$.

**Table** 3.3: Adjusted resistance parameters.

| Parameter | Value |
|---|---|
| $\eta_1$ | -2.6e02 |
| $\eta_2$ | 6.44 |
| $\eta_3$ | -0.04 |
| $\eta_4$ | 1.4e-04 |
| $\eta_5$ | -2.1e-07 |
| $\eta_6$ | 1.6e-10 |
| $\eta_7$ | -5.3e-14 |
| $\eta_8$ | 5.7e-18 |

The level comparison MSE with and without the adjusted fluid resistance can be seen in Table 3.4. There is a MSE reduction with the adjusted fluid resistance.

**Table** 3.4: Mean squared error (MSE).

| MSE | Value |
|---|---|
| Without adjustment | 1.3646 |
| With adjustment | 1.0692 |

Figure 3.5 shows the comparison between $u$ and $\hat{u}$. The experimental resistance calculated from the gate position is is pretty close to the adjusted resistence.

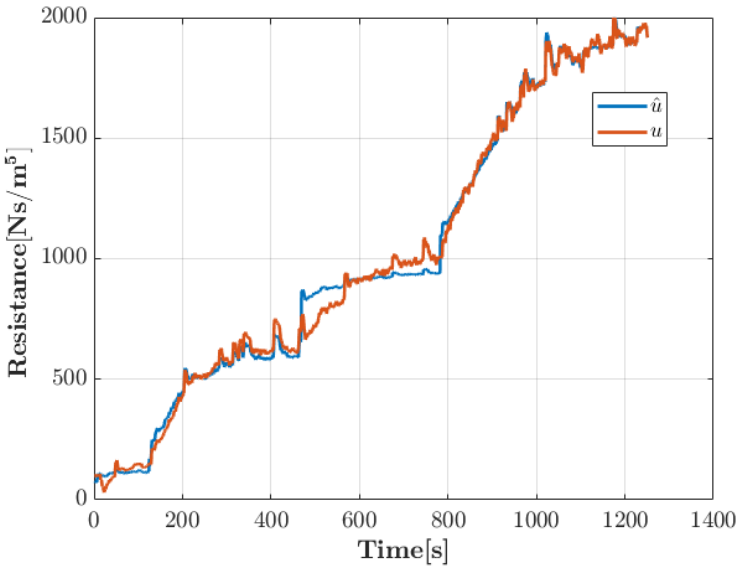


**Figure** 3.5: Fluid resistance comparison between $\hat{u}$ and $u$.

Figure 3.6 shows the water height level experimental validation. Due to the similarities between the experimental and the adjusted resistance the comparison between the model tank and the experimental water height level are very closer between them.

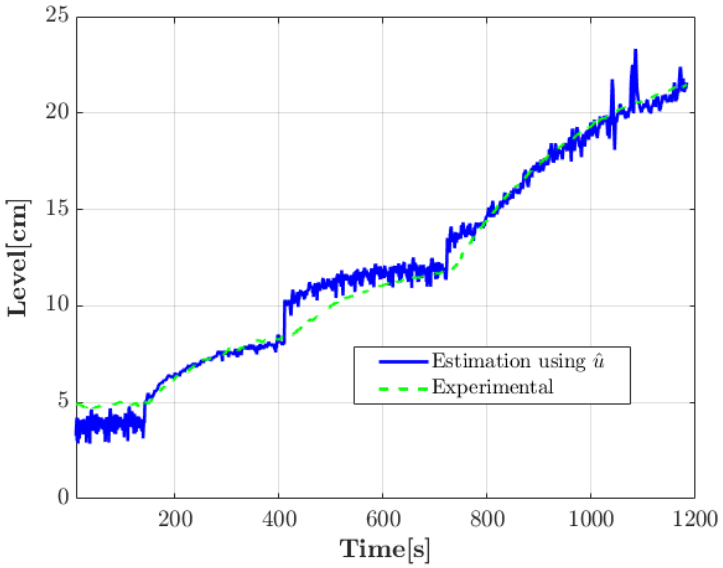


**Figure** 3.6: Experimental and model water height level validation.

With the identified micro-channel model parameters a control law can be designed to control the water height level inside the micro-channel.

## 3.4 Summary

In order to get an accurate model that represents the dynamics of a micro-channel experimental plant, an identification process has to be done to obtain the model parameters that are difficult to measure. Two types of interconnected subsystems were identified. The first subsystem considers an uncontrollable resistance. The second subsystem considers a controllable resistance that represents the sluice gate position.The interconnection of two subsystems with uncontrollable resistances and one subsystem with a controllable resistance is used to validate the subsystems identified.

The capacitance was calculated based on the geometric micro-channel characteristics, being constant for all the subsystems. The inertance and the uncontrollable resistance were identified. The theoretical PHS structure is adjusted with the experimental setup through a parameter identification experiment using OLS. A PRBS signal is used to manipulate the sluice gate position. The estimation using three basic elements shows some error between the estimated water height level and the experimental data. To improve the estimation the fluid resistance was further adjusted. In this chapter three subsystems were interconnected. In the next chapters four subsystems are interconnected to better approximate the process and its control and to cover all the micro-channel length.

# 4. CONTROLLER DESIGN BASED ON THE TOTAL HYDRAULIC-MECHANICAL ENERGY AS A LOCAL LYAPUNOV FUNCTION

## 4.1 Introduction

In irrigation channels the objective is to maintain a constant level in a pool. This level decreases until the last pool has the best use of the water. A proportional controller to maintain a desired level was designed, bounding the total energy through the potential energy. To have a better approximation of the pool, the controller has to control the volume of an upstream tank, modifying the value of the resistance corresponding to a downstream pipe's gate. According to the basic element interconnection model approach in [38] a proportional control law based on the total hydraulic-mechanical energy as a local Lyapunov function was presented. The proportional control has some advantages such as to be easy to design, to present a quick response and to be stable. This proportional controller is simulated and implemented in the experimental setup. The following proposition presents the controller.

## 4.2 Controller design

**Proposition 4.2.1.** Consider the subindex $\mathrm{N}$ to denote the tank subsystem just before the controllable fluid resistance. Then the control law

$$u = \frac{\beta \mathrm{I_N}(\Pi_\mathrm{N} - \Pi_\mathrm{N}^*)}{q_\mathrm{N}} - \frac{\delta(V_\mathrm{N} - V_\mathrm{N}^*)}{\alpha \mathrm{C_{fN}} q_\mathrm{N}} + \frac{(p_\mathrm{N} - p_{ext})}{q_\mathrm{N}} \tag{4.1}$$

with $V_\mathrm{N}^*$ the volume reference, $\Pi_\mathrm{N}^* = \mathrm{I_N} q_\mathrm{N}^*$ the corresponding steady state momentum and with $\delta, \alpha, \beta$ positive tuning constants.

*Proof.* Consider the following local energy function for the $\mathrm{N}$-th section

$$H_{d_\mathrm{N}} = \frac{\delta}{2} \frac{(V_\mathrm{N} - V_\mathrm{N}^*)^2}{\mathrm{C_{f_N}}} + \frac{\alpha}{2} \frac{(\Pi_\mathrm{N} - \Pi_\mathrm{N}^*)^2}{\mathrm{I_N}} \tag{4.2}$$

Considering a constant input flow, its time derivative is

$$\dot{H}_{d_\mathrm{N}} = \frac{\delta(V_\mathrm{N} - V_\mathrm{N}^*)}{\mathrm{C_{f_N}}}(q_{\mathrm{N}-1} - q_\mathrm{N}) + \frac{\alpha(\Pi_\mathrm{N} - \Pi_\mathrm{N}^*)}{\mathrm{I_N}}(p_\mathrm{N} - p_{ext} - u q_\mathrm{N}) \tag{4.3}$$

Considering the equilibrium point, we have $\frac{\Pi_\mathrm{N}^*}{\mathrm{I_N}} = q_{\mathrm{N}-1}$ and that $\frac{\Pi_\mathrm{N}}{\mathrm{I_N}} = q_\mathrm{N}$, then we have

$$\dot{H}_{d_\mathrm{N}} = -\frac{\delta(V_\mathrm{N} - V_\mathrm{N}^*)}{\mathrm{C_{f_N} I_N}}(\Pi_\mathrm{N} - \Pi_\mathrm{N}^*) + \frac{\alpha(\Pi_\mathrm{N} - \Pi_\mathrm{N}^*)}{\mathrm{I_N}}(p_\mathrm{N} - p_{ext} - u q_\mathrm{N}) \tag{4.4}$$

Replacing (4.1) in (4.4) we get

$$\dot{H}_{d_\mathrm{N}} = -\alpha\beta(\Pi_\mathrm{N} - \Pi_\mathrm{N}^*)^2 \leq 0 \tag{4.5}$$

from where we get asymptotic stability applying LaSalle's invariance principle. ■

Observe that that the controller defined by (4.1) is proportional to the first two terms, which are related to the pressure momentum error $\Pi_{\mathrm{N}} - \Pi_{\mathrm{N}}^{*}$ and the volume error $V_{\mathrm{N}} - V_{\mathrm{N}}^{*}$.

## 4.3 Simulations

To probe the controller performance twenty tanks are considered for this simulation, the model parameters are obtained from the geometric characteristics from the micro-channel, in the next section the identified parameters are used in the controller implementation. The water height level of the first tank is controlled manipulating the resistance (sluice gate) of the tenth pipe, and the level of the eleventh tank is set by the last resistance. The set point level is twenty five centimeters for the first tank and eighteen centimeters for the eleventh tank. The control is activated at $t = 200s$. A change in the input from $5l/s$ to $6l/s$ at the time $t = 300s$ allows us to observe the response of the controller with a perturbation. Two cases are explored, when the resistance between tanks is $\mathrm{R_{fn}} = 10Ns/m^5$ and $\mathrm{R_{fn}} = 0.01Ns/m^5$. And the tuning constants $\alpha_n = 0.5$, $\beta_n = 190$ and $\delta_{\mathrm{n}} = 0.17$. The simulations have the next parameters: $\mathrm{C_{f_n}} = 0.0015m^5/N$, $\mathrm{I_n} = 0.3401Ns^2/m^5$, $q_{in} = 5l/s$, After a perturbation the level stabilizes to the set point in both tanks. To get this, the resistances increase their values to raise the volumes of all the tanks. The first and eleventh tank get to the set point also with a change of the input flow.

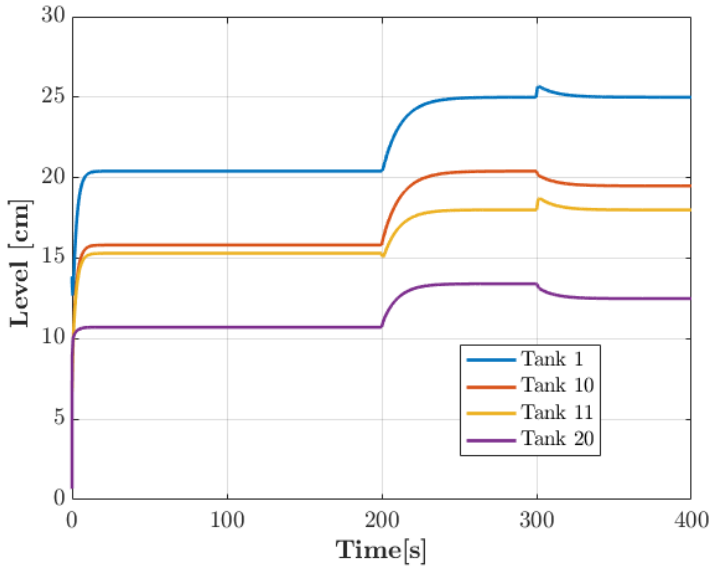


**Figure** 4.1: Level of two pools of the micro-channel considering two groups of ten tanks and pipes interconnected with a set point of twenty five centimeters in the first tank, and eighteen centimeters in the eleventh tank. Considering a $\mathrm{Rf_n} = 10Ns/m^5$ between the tanks.

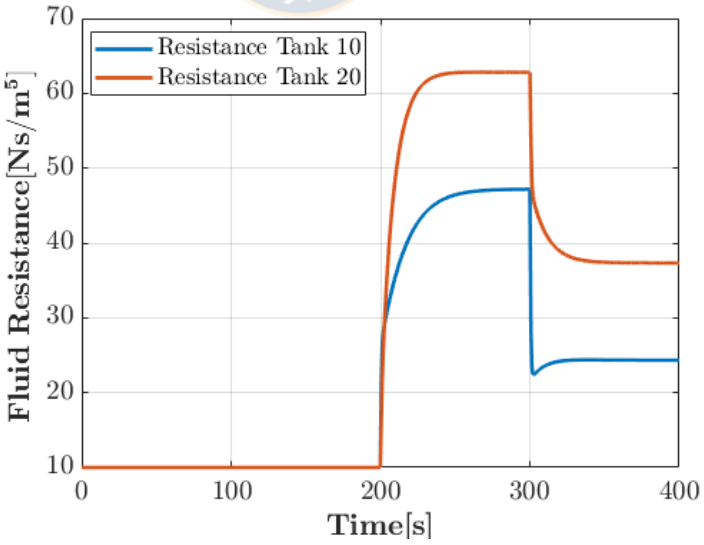


**Figure** 4.2: Resistance of two pools of the micro-channel considering two groups of ten tanks and pipes interconnected with a set point of twenty five centimeters in the first tank, and eighteen centimeters in the eleventh tank. Considering a $\mathrm{Rf_n} = 10Ns/m^5$ between the tanks.

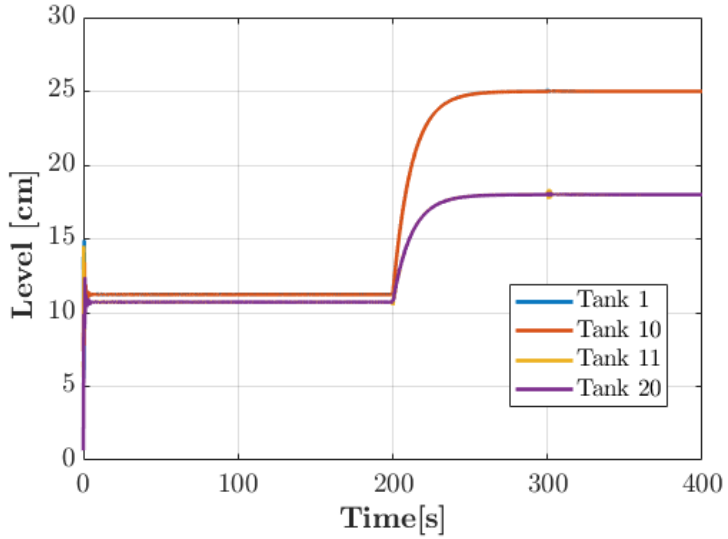


**Figure** 4.3: Level of two pools interconnected of the micro-channel considering two groups of ten tanks and pipes with a set point of twenty five centimeters in the first tank and eighteen centimeters in the eleventh tank. Considering a $\mathrm{Rf_n} = 0.01 Ns/m^5$ between the tanks.

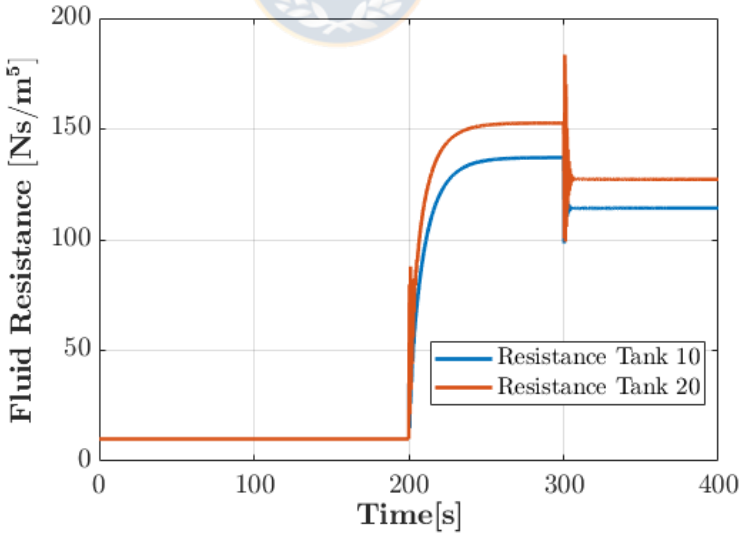


**Figure** 4.4: Resistance of two pools interconnected of the micro-channel considering two groups of ten tanks and pipes with a set point of twenty five centimeters in the first tank and eighteen centimeters in the eleventh tank. Considering a $\mathrm{Rf_n} = 0.01 Ns/m^5$ between the tanks.

In the second case the changes in the input flow cause smaller changes than the first case, but the control effort is greater than the first case. The control resistance in the second case presents oscillations due the flow when the resistance between the tanks is small. See Figures 4.1, 4.2, 4.3, 4.4. The steady state error is zero due the selection of the desired pressure momentum equal the pressure momentum of the previous tanks. Without this selection the simulations will present steady state error. To correct for any selection of desired pressure momentum, an integrator should be added.

### 4.3.1 Experimental control validation

In this experimental validation four subsystems were considered to represent the micro-channel. The plant dynamics are extremely slow for this reason the sampling time used by the controller does not affect its performance. The controller was implemented in MATLAB® - Simulink ® . The solver type is : variable step. The controller is connected with the PLC by an interface developed in Spyder-Python ® (https://www.spyder-ide.org/) with a sample time of $0.1s$. The parameters used were obtained from the identification experiment in Chapter 3: $\mathrm{R_{fn}} = 22.5Ns/m^5$, the fluid capacitance for each tank is $\mathrm{C_{fn}} = 0.0195m^5/N$, the fluid inertance for all the pipes is $\mathrm{I_n} = 4.6Ns^2/m^5$ and the inertance for the last pipe is $\mathrm{I_4} = 0.0294Ns^2/m^5$. The level set-point is $16cm$ at $35s$. The sub-index of the pipes are related with the number of system, being $\mathrm{N}$ the last subsystem, $n = 1, 2, 3, ..., \mathrm{N}$

The Table 4.1 shows the control tuning constants used in this control validation experiment.

**Table** 4.1: Tuning control constants.

| Tuning constant | Value | Tuning constant | Value | Tuning constant | Value |
|---|---|---|---|---|---|
| $\alpha$ | 0.00025 | $\beta$ | 11 | $\delta$ | 0.005 |

Figure 4.5 shows the simulated water level height in the first tank. The set-point is $16cm$. The controller gets the desired level after $800s$. The first subsystem water level height does not present steady state error.

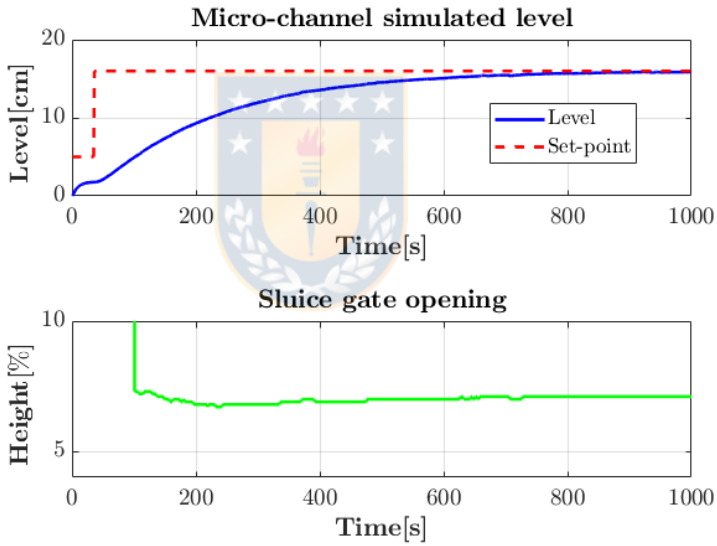


**Figure** 4.5: Simulated water level height.

The experimental results are shown in Figure 4.6. The first tank water level height presents steady state error caused by the model, the gate errors and other perturbations.

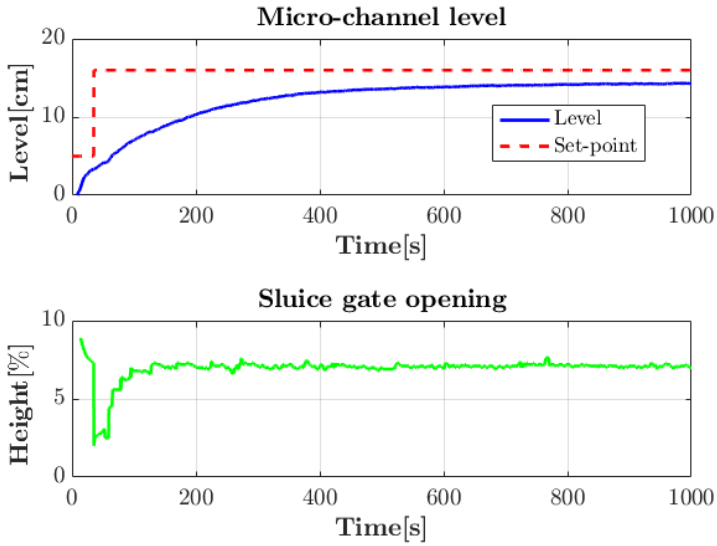


**Figure** 4.6: Experimental water level height.

The error between the experimental and the set-point water level height is approximately of $1cm$. To correct the steady state error an integral action should be added.

## 4.4 Summary

The level of a determined tank can be controlled manipulating the value of resistance (position of the gate) of the last pipe. The controller designed using the total hydraulic-mechanical energy as a local Lyapunov function can be interpreted as a proportional control.

The developed controller requires an accurate model due the model is used to estimate heights and flows that are not measured to determine the appropriate gate position. A MATLAB® - Simulink ® program was used to link the developed controller with the experimental setup.

The experimental results show steady state error caused by the uncertainties of the micro-channel and the gate models and other perturbations. The steady state error could be rejected by the addition of an integral action.

# 5. Level controlller design adding integral action

## 5.1 Introduction

The integral action (IA) is applied to mitigate different phenomena such as constant disturbance inputs or model uncertainties. The work proposed by [48] reviews the fundamental theory, main results and practical applications of passive based control (PBC), where an integrator can be added around the passive output preserving stability. Based on the work aforementioned, [49] presents a technique to get an IA on system variables having relative degree higher than one, preserving the Hamiltonian form and the closed loop stability, the design procedure was proved in a permanent magnet synchronous motor (PMSM) loaded with unknown constant torque to reject constant disturbances and improve control system robustness. A set of algebraic equations must be solved to find a change of variables that allows to build an extended PCHD preserving the form of the Hamiltonian function and the characteristic matrices of the original port controlled Hamiltonian systems with dissipation (PCHD).

The design of robust integral control of PHS with non-passive outputs with unmatched disturbances (the disturbances may not be matched with the input) is shown in [50], classical examples are mechanical systems and electrical motors where the passive outputs are velocities and currents, respectively, but the output of interest is often position. In [26] the same problem is attacked, but the control is made by interconnection of PHS, the procedure proposed avoids a change of coordinates keeping the original state vector, which contains variables with physical interpretation. The application chosen for this procedure is an electrical circuit and a PMSM.

In [51] a method to design a set-point regulation controller with integral action is proposed and applied to under actuated robotic system, the control design is based on a coordinate transformation and a dynamic extension, where the robot is described as a PHS. Some works deals with the problem to design robust proportional integral PI (RPI), focuses in nonlinear systems [52] oriented to temperature regulation. Integral interconnection and damping assignment passivity based control (IDA-PBC) and proportional integral derivative (PID) for PHS is addressed in [53], that allows the implementation of integral action control to under-actuated PCH systems that are quite commonly found in practice. The results are applied to control a Quanser inertia wheel pendulum.

The work developed by [54] presents a method for the addition of IA to non passive outputs of a class of PHS, where the controller is able to reject the effects of matched and unmatched disturbances, preserving the regulation of the non-passive outputs. The methodology proposed is illustrated on an electrical circuit and on a PMSM. The control law proposed is given explicitly, without the need of coordinate transformation. A PID controller is designed to stabilize a PHS, the design is based on passivity theory [55]. The design of an integral control in the current loop of a PMSM based on passivity is explained in [56]. Experimental simulation results show that the proposed control strategy can effectively suppress the constant and time-varying disturbances, eliminate the steady-state error, and improve the robustness of the system. Other applications in a Y- connected modular multilevel converter for fractional frequency transmission using IDA-PB control with integral action is explored in [57]. Three typical IDA-PBC strategies are then proposed, featuring the asymptotical stability of the desired equilibrium. To eliminate steady-state error, integrators are further added to the IDA-PB controller and a robust IDA-PBC based load voltage controller for power quality enhancement of standalone microgrids as proposed in [58].

## 5.2 Integral Action Controller (IAC)

To correct any steady state error an integral action controller is implemented to determine the dynamic fluid resistance. Our system has a nonpassive output i.e. the integral action can not be applied via a dynamic extension because is no a control input acting on the variable of primary interest $V_1$.

We are motivated by the CBI developed in [54]. The authors of [54] apply an IAC on a RLC circuit model to reject the unmatched disturbances. The control objective variable is the volume $V_1$ because we want to get a desired height in the micro-channel.

For the design of the IAC we assume that the system is operating at some constant equilibrium, determined by a constant input flow and outside pressure. The controller is designed to assure that the volume $V_{\mathrm{N}}$ of of subsystem $\mathrm{N}$ is kept at some desired value $V_{\mathrm{N}}^*$ in the presence of parameter uncertainties or slow changes in the input flow of the system or exterior pressure of the system. Rewriting the model of the micro-channel as an input affine control system, considering constant disturbances and with respect to a shifted Hamiltonian function with its minimum a the desired dynamic equilibrium we have

$$\begin{bmatrix} \dot{V}_1 \\ \dot{\Pi}_1 \\ \dot{V}_2 \\ \dot{\Pi}_2 \\ \vdots \\ \dot{V}_{\mathrm{N}} \\ \dot{\Pi}_{\mathrm{N}} \end{bmatrix} = \begin{bmatrix} 0 & -1 & 0 & \cdots & 0 & 0 \\ 1 & -\mathrm{R}_{\mathrm{f}_1} & -1 & \cdots & 0 & 0 \\ 0 & 1 & 0 & \cdots & 0 & 0 \\ 0 & 0 & 1 & \cdots & 0 & 0 \\ \vdots & \vdots & \vdots & \ddots & \vdots & \vdots \\ 0 & 0 & 0 & \cdots & 0 & -1 \\ 0 & 0 & 0 & \cdots & 1 & -\mathrm{R}_{\mathrm{f}_{\mathrm{N}}} \end{bmatrix} \begin{bmatrix} \nabla_{V_1} H_d \\ \nabla_{\Pi_1} H_d \\ \nabla_{V_2} H_d \\ \nabla_{\Pi_2} H_d \\ \vdots \\ \nabla_{V_{\mathrm{N}}} H_d \\ \nabla_{\Pi_{\mathrm{N}}} H_d \end{bmatrix} + \begin{bmatrix} 0 & 0 & 0 & 0 & \cdots & 0 & 1 \end{bmatrix}^\top u \quad (5.1)$$

with conjugated output $y = q_{\mathrm{N}}$. It is assumed that the controlled gate, at the exit of tank system $\mathrm{N}$, is newer completely closed.This is accounted for by the constant fluid resistance $\mathrm{R}_{\mathrm{f}_{\mathrm{N}}}$. The shifted Hamiltonian function is

$$\begin{aligned} H_d =& \frac{1}{2\mathrm{C}_{\mathrm{f}_1}}(V_1 - V_1^*)^2 + \frac{1}{2\mathrm{I}_1}(\Pi_1 - \Pi_1^*)^2 + \cdots \\ &+ \frac{1}{2\mathrm{C}_{\mathrm{f}_{\mathrm{N}}}}(V_{\mathrm{N}} - V_{\mathrm{N}}^*)^2 + \frac{1}{2\mathrm{I}_{\mathrm{N}}}(\Pi_{\mathrm{N}} - \Pi_{\mathrm{N}}^*)^2 \end{aligned} \tag{5.2}$$

where the equilibrium point $(V^*, \Pi^*)$ is function of the constant input flow $q_{in}^*$, constant exterior pressure $p_{ext}^*$ and the slope drop pressures $p_{\Delta}^*$. Just as in the previous section, a local controller, i.e. a controller for the $\mathrm{N}$-th tank system section, is synthesized in order to control the level around the section at some reference value. Considering the $\mathrm{N}$-th section we have

$$\begin{aligned} \begin{bmatrix} \dot{V}_{\mathrm{N}} \\ \dot{\Pi}_{\mathrm{N}} \end{bmatrix} =& \begin{bmatrix} 0 & -1 \\ 1 & -\mathrm{R}_{\mathrm{f}_{\mathrm{N}}} \end{bmatrix} \begin{bmatrix} \nabla_{V_{\mathrm{N}}} H_{d_{\mathrm{N}}} \\ \nabla_{\Pi_{\mathrm{N}}} H_{d_{\mathrm{N}}} \end{bmatrix} + \begin{bmatrix} 0 \\ 1 \end{bmatrix} u - \begin{bmatrix} 0 \\ 1 \end{bmatrix} \mathrm{d}_1 - \begin{bmatrix} 1 \\ 0 \end{bmatrix} \mathrm{d}_2 \\ y =& q_{\mathrm{N}} \end{aligned} \tag{5.3}$$

where $H_{d_{\mathrm{N}}}$ is the Hamiltonian of section $\mathrm{N}$ and $\mathrm{d}_1$ and $\mathrm{d}_2$ are constant disturbances which take into account any constant or very slow variation in the inlet flow and parameter modelling errors which are propagated through the model. The considered integral PHS controller is

$$\begin{aligned} \dot{\zeta} =& \frac{(V_{\mathrm{N}} - V_{\mathrm{N}}^*)}{\mathrm{C}_{\mathrm{f}_{\mathrm{N}}}} \\ u =& -\frac{\mathrm{R}_{\mathrm{f}_{\mathrm{N}}}}{\mathrm{I}_{\mathrm{a}}}(\Pi_{\mathrm{N}} - \zeta) \end{aligned} \tag{5.4}$$

where $\zeta \in \mathbb{R}$ is the state of the controller, $H_c(\Pi_{\mathrm{N}}, \zeta) = \frac{1}{2\mathrm{I}_{\mathrm{a}}}(\Pi_{\mathrm{N}} - \zeta)^2$ is the controller Hamiltonian function and $\mathrm{I}_{\mathrm{a}}$ is a positive tuning constant to be selected. The closed loop

dynamic is then given by

$$\begin{bmatrix} \dot{V}_{\mathrm{N}} \\ \dot{\Pi}_{\mathrm{N}} \\ \dot{\zeta} \end{bmatrix} = \begin{bmatrix} 0 & -1 & -1 \\ 1 & -\mathrm{R}_{\mathrm{f_N}} & 0 \\ 1 & 0 & 0 \end{bmatrix} \begin{bmatrix} \nabla_{V_{\mathrm{N}}} H_{cl} \\ \nabla_{\Pi_{\mathrm{N}}} H_{cl} \\ \nabla_{\zeta} H_{cl} \end{bmatrix} - \begin{bmatrix} 0 \\ 1 \\ 0 \end{bmatrix} \mathrm{d}_1 - \begin{bmatrix} 1 \\ 0 \\ 0 \end{bmatrix} \mathrm{d}_2 \tag{5.5}$$

where the closed-loop Hamiltonian is given by

$$H_{cl} = H_{d_{\mathrm{N}}} + H_c \tag{5.6}$$

The control system (5.4) allows regulate the volume reference $V_{\mathrm{N}}$ by adjusting the reference value of the momentum coordinate. The reader is refereed to [54] for further details. The following assumption is necessary to guarantee closed-loop asymptotic stability.

**Assumption 5.2.1.** $\mathrm{R}_{\mathrm{f_N}}$ *is constant,* $H_{d_{\mathrm{N}}}$ *is strongly convex and have no cross terms between* $\Pi_{\mathrm{N}}$ *and* $V_{\mathrm{N}}$*, and there is an equilibrium point of* $\Pi_{\mathrm{N}}$ *such that* $\nabla_{\Pi_{\mathrm{N}}} H_d = -\mathrm{d}_2$.

Under Assumption 5.2.1 the closed-gradient at equilibrium becomes

$$\begin{bmatrix} \nabla_{V_{\mathrm{N}}} H^*_{cl} \\ \nabla_{\Pi_{\mathrm{N}}} H^*_{cl} \\ \nabla_{\zeta} H^*_{cl} \end{bmatrix} = \begin{bmatrix} 0 \\ -\mathrm{R}^{-1}_{\mathrm{f_N}} \mathrm{d}_1 \\ \mathrm{R}^{-1}_{\mathrm{f_N}} \mathrm{d}_1 - \mathrm{d}_2 \end{bmatrix} \tag{5.7}$$

implying that the desired reference $V^*_{\mathrm{N}}$ is assured by shifting the closed-equilibrium for the $\Pi_{\mathrm{N}}$ coordinate.

**Proposition 5.2.1.** If Assumption 5.2.1 is satisfied then the closed-loop system (5.7) is asymptotically stable.

*Proof.* The proof follows by direct application of Proposition 3 in [54] considering as

Lyapunov function

$$W = H_{cl}(w) - [w - w^*]^\top \nabla H_{cl}(w^*) - H_{cl}(w^*) \tag{5.8}$$

where $w = [\Pi_{\mathrm{N}}, V_{\mathrm{N}}, \zeta]^\top$.

■

The dynamic controller can be interpreted as the interconnection of a fluid Resistance-Inertance parallel circuit in series with a pressure source as shown in Figure 5.1. Since the controllable fluid resistance $\mathrm{R}_{\mathrm{f_N}}$ is part of the control action it appears as part of the controller in the figure. The fluid inertance $\mathrm{I_a}$ is connected in parallel with $\mathrm{R}_{\mathrm{f_N}}$ and the desired pressure reference is obtained by a pressure source of value $\mathrm{V}^*_{\mathrm{N}}/\mathrm{C}_{\mathrm{f_N}}$.

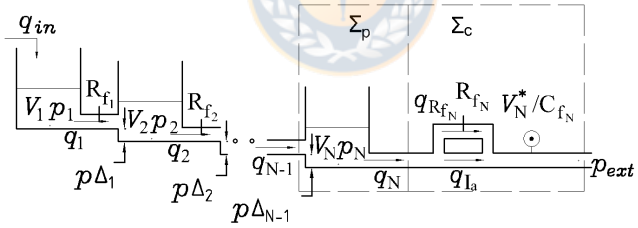


**Figure** 5.1: Micro-channel model with integral action.

Figure 5.1 shows that the control action can be interpreted as the interconnection of the last section of the tank system with the dynamic controller. Indeed, it is not difficult to show that (5.4) can be written as the equivalent system

$$\begin{aligned} \dot{z} &= -\,\mathrm{R}_{\mathrm{f_N}} \nabla_z H_c - \mathrm{R}_{\mathrm{f_N}} u_c - p_{ext} \\ u &= -\,\frac{\mathrm{R}_{\mathrm{f_N}}}{\mathrm{I_a}} z - \mathrm{R}_{\mathrm{f_N}} u_c \end{aligned} \tag{5.9}$$

using coordinate transformation $z = \Pi_{\mathrm{N}} - \zeta$, and where $u_c$ is the input of the controller.

The closed-loop system is then obtained by a power preserving interconnection between (5.9) and (5.3). See [54] for more details on the interpretation of this class of control system.

## 5.3 Simulations and experiment

Four tanks were considered for this simulation. The level of the first tank is controlled manipulating the resistance (gate) of the fourth pipe. The control is activated at $t = 100s$. The resistance between tanks is $\mathrm{R_{fn}} = 22.5Ns/m^5$. The fluid capacitance for each tank is $\mathrm{C_{fn}} = 0.0195m^5/N$, the fluid inertance for all the pipes is $\mathrm{I_n} = 4.6Ns^2/m^5$. The inertance for the last pipe is $\mathrm{I_N} = 0.0294Ns^2/m^5$. The selected controller constants are $\mathrm{I_a} = 750Ns^2/m^5$ and $\mathrm{R_a} = 4.9\mathrm{Ns/m^5}$. The sub-index of the pipes are related with the number of system, being N the last subsystem, $n = 1, 2, 3, ..., \mathrm{N}$

Figure 5.2 shows the integral controller simulations. The controller is activated at $100s$. The set-point is $16cm$. The water height level gets the set-point after $500s$. The water height level is disturbed by a $2\%$ increment in the input flow at $1000s$. The water height level is regulated by the integral controller getting the set-point approximately at $1500s$.

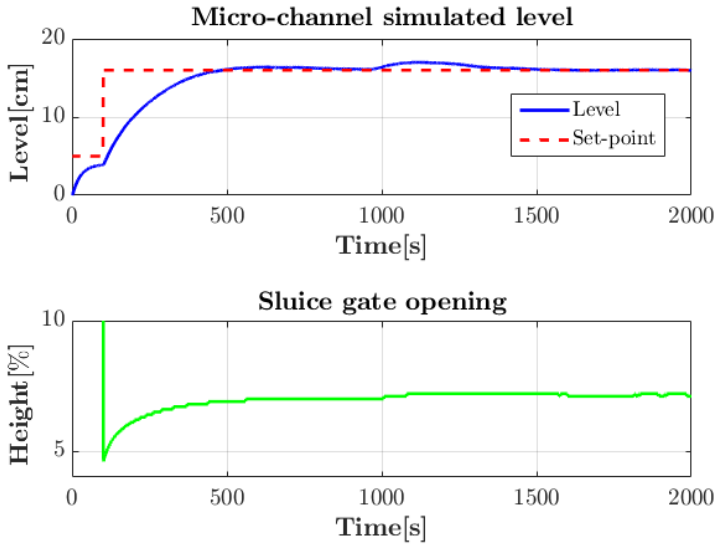


**Figure** 5.2: Simulated level with IA

Figure 5.3 shows the experimental results. The controller is activated at $100s$. The desired water height level is $16cm$. The micro-channel height level gets the set-point after $500s$. The controller can maintain the desired level even with an input flow increment of $2\%$ at $1000s$.

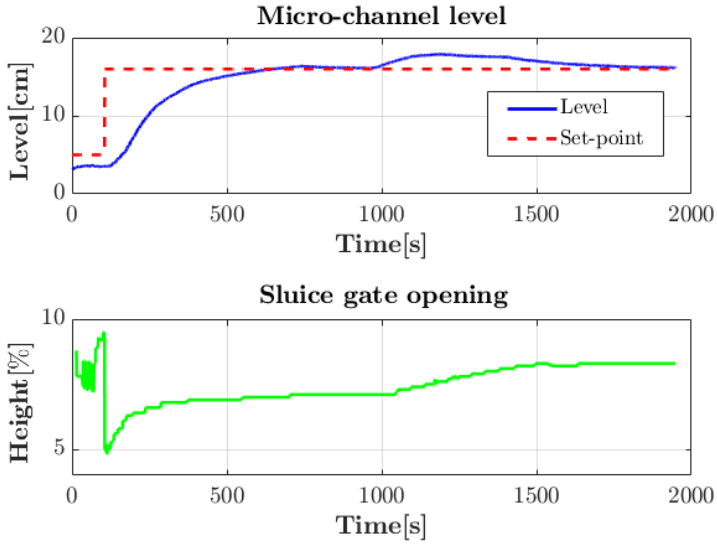


**Figure** 5.3: Experimental level with IA

Comparing Figures 5.2 and 5.3 we can observe that the simulation response is similar to the experimental results. The opening sluice gate is slightly different between the simulation and the experimental results.

## 5.4 Summary

The IAC is a direct application of a of the integral action scheme as control of interconnection (CbI). The simulations results show that the IA implemented avoided the steady state error caused by the model and the gate position. The IA controller can correct input flow changes. The product between the control output and the input map allows to access only to the first variable. We consider the fluid resistance $\mathrm{R_a}$ as part of the controller. The controller (5.4) can be interpreted as a proportional-integral (PI) controller with a output flow proportional term and an integral term. The pressure drop that represents the slope can be seen as an unmatched disturbance.

# 6. CONCLUSIONS

## 6.1 Contributions

The main contribution of this thesis is the representation of a micro-channel by a fluid-structure interconnected system. This fluid-structure interconnected system is formed by several subsystems. Each subsystem has a fluid capacitance, a fluid inertance and a fluid resistance. There are two types of subsystems differentiated by the presence of an uncontrollable or a controllable fluid resistance. The controllable fluid resistance represents the actuator (in this case a sluice gate). The entire structure has several subsystems with uncontrollable fluid resistances but the subsystem with the controllable fluid resistance is located at the sluice gates.

## 6.2 Conclusions

The proposed interconnected model is based on basic elements (subsystems) that can represent the micro-channel behavior within the PHS framework. The total energy equation is divided in two parts, being the sum of the potential energy related with the energy stored in a tank and the kinetic energy caused by the fluid movement through a pipe.

The micro-channel model parameters obtained from the PHS formulation was identi-

fied to be used to estimate variables and to deduce a control law. The fluid capacitance can be obtained from the channel dimensions, but the parameters related with the fluid inertance and the uncontrollable resistance are more difficult to identify. To identify the micro-channel parameters an experiment based on OLS was performed. We choose a micro-channel section divided in two parts. Each part represented a different subsystem type.

We identified the fluid inertances and the uncontrollable fluid resistances whilst the fluid capacitance was identified from the geometric characteristics of the micro-channel. The validation was done with the interconnection of three subsystems. We interconnect two subsystems with uncontrollable resistance and one subsystem with controllable resistance. After the identification process a resistance adjustment was done to improve the micro-channel model approximation. We use four subsystems to deduce the control law. The idea is to interconnect several identified subsystems to model a channel.

A controller based on four subsystems interconnection model was designed. This controller is based on a local Lyapunov equation. The simulations shown good results, whilst the experimental results presented steady state error. The steady state error is caused by slight micro-channel and gate modelling errors. The control developed here can be interpreted as a proportional control. The control based on a local Lyapunov equation has some advantages such as to be easy to design, to present a quick response and to be stable. The disadvantages are: the controller can not reject disturbances and the controller needs an accurate model.

To correct the steady state error an IAC was implemented. The controller could then correct the steady state error even with an input flow disturbance. The IAC controller is inspired by the CBI robust controller. The PHS micro-channel model presents nonpassive outputs i.e. we do not have access to the primary interest variable. The IAC shown in this

thesis allow us to control the volume $V_1$ to have a desired water level height manipulating the opening sluice gate that we interpreted as a dynamic resistance value that modifies the output flow.

From the experiments we conclude that the plant delays associated with the actuators are negligible compared with the plant dynamics.

## 6.3 Future research

Future research could be focused in the analysis of other identification methods to improve the identification results.

In future experiments new subsystems with reduced dimensions could be identified to demonstrate a better approximation to the dynamics of the micro-channel with the interconnection of a large number of them.

Multiple controllers based on the hydraulic-mechanical equations could be implemented to observe their performance dividing the micro-channel in several pools. The same implementation could be done for the IAC controller. Depending of the required precision, a combination of controllers could be implemented in different pools of the same micro-channel.

# Bibliography


[1] R. Ortega, A. J. Van Der Schaft, I. Mareels, and B. Maschke, "Putting energy back in control," *IEEE Control Systems Magazine*, vol. 21, no. 2, pp. 18–33, April 2001.

[2] A. van der Schaft and D. Jeltsema, *Port-Hamiltonian Systems Theory: An Introductory Overview*, 2014.

[3] I. Calle, *Modelamiento Y Control De Sistemas Físicos Usando El Enfoque Port-Hamiltoniano*, 2010.

[4] S. P. Nageshrao, G. A. D. Lopes, D. Jeltsema, and R. Babuška, "Port-Hamiltonian Systems in Adaptive and Learning Control: A Survey," *IEEE Transactions on Automatic Control*, vol. 61, no. 5, pp. 1223–1238, May 2016.

[5] A. van der Schaft, *L2-Gain and Passivity Techniques in Nonlinear Control*, 3rd ed. Springer Publishing Company, Incorporated, 2016.

[6] D. Rowell and D. N. Wormley, *System dynamics : an introduction*. Upper Saddle River, NJ : Prentice Hall, 1997.

[7] D. Sbarbaro and R. Ortega, "Averaging level control: An approach based on mass balance," *Journal of Process Control*, vol. 17, no. 7, pp. 621 – 629, 2007.

[8] B. Hamroun, L. Lefevre, and E. Mendes, "Port-based modelling and geometric reduction for open channel irrigation systems," in *2007 46th IEEE Conference on Decision and Control*, Dec 2007, pp. 1578–1583.

[9] V. Te Chow, *Open-channel hydraulics*, ser. McGraw-Hill civil engineering series. McGraw-Hill, 1959.

[10] J. C. Willems, "Paradigms and puzzles in the theory of dynamical systems," *IEEE Transactions on Automatic Control*, vol. 36, no. 3, pp. 259–294, 1991.

[11] M. Takegaki and S. Arimoto, "A new feedback method for dynamic control of manipulators," *Journal of Dynamic Systems Measurement and Control-transactions of The Asme - J DYN SYST MEAS CONTR*, vol. 103, 06 1981.

[12] E. Jonckheere, "Lagrangian theory of large scale systems," in *Lagrangian theory of large scale systems*, vol. 102, 1981, pp. 119–125.

[13] R. Ortega and M. W. Spong, "Adaptive motion control of rigid robots: A tutorial," *Automatica*, vol. 25, no. 6, pp. 877 – 888, 1989.

[14] V. Petrovic, R. Ortega, A. Stankovic, and G. Tadmor, "Design and implementation of an adaptive controller for torque ripple minimization in pm synchronous motors," *Power Electronics, IEEE Transactions on*, vol. 15, pp. 871 – 880, 10 2000.

[15] H. Berghuis and H. Nijmeijer, "A passivity approach to controller-observer design for robots," *IEEE transactions on robotics and automation*, vol. 9, no. 6, pp. 740–754, 1993.

[16] L. Lanari and J. Wen, "Asymtotically stable set point control laws for flexible robots," *Systems and Control Letters*, vol. 19, pp. 119–129, 08 1992.

[17] R. Prasanth and R. Mehra, "Nonlinear servoelastic control using Euler-Lagrange theory," *in Proceedings of the International Conference American Institute Aeronautics and Astronautics*, vol. 39, pp. 837–847, 1999.

[18] R. Akmeliawati and I. Mareels, "Flight control systems using passivity-based control - disturbance rejection and robustness analysis," *Guidance, Navigation, and Control Conference and Exhibit,American Institute of Aeronautics and Astronautics*, vol. 45, 1999.

[19] B. Maschke, R. Ortega, and A. J. Van Der Schaft, "Energy-based Lyapunov functions for forced Hamiltonian systems with dissipation," *IEEE Transactions on Automatic Control*, vol. 45, no. 8, pp. 1498–1502, Aug 2000.

[20] R. Ortega, A. van der Schaft, B. Maschke, and G. Escobar, "Energy-shaping of port-controlled Hamiltonian systems by interconnection," in *Proceedings of the 38th IEEE Conference on Decision and Control (Cat. No.99CH36304)*, vol. 2, Dec 1999, pp. 1646–1651 vol.2.

[21] R. Ortega, A. van der Schaft, B. Maschke, and G. Escobar, "Interconnection and damping assignment passivity-based control of port-controlled Hamiltonian systems," *Automatica*, vol. 38, no. 4, pp. 585 – 596, 2002.

[22] R. Ortega, A. Astolfi, G.Bastin, and H. Rodriguez, "Output-feedback regulation of mass-balance systems," *in New Directions in Nonlinear Observer Design, H.Nijmeijer and T. Fossen, Eds. Berlin, Germany: Springer-Verlag*, 1999.

[23] V. Petrovic, R. Ortega, and A. M. Stankovic, "A globally convergent energy-based controller for pm synchronous motors," in *Proceedings of the 38th IEEE Conference on Decision and Control (Cat. No.99CH36304)*, vol. 1, Dec 1999, pp. 334–340 vol.1.

[24] M. Galaz, R. Ortega, A. Bazanella, and A. Stankovic, "An Energy-Shaping Approach to Excitation Control of Synchronous Generators," *Automatica*, vol. 39, pp. 111–119, 01 2003.

[25] H. Rodriguez, R. Ortega, and I. Mareels, "Nonlinear control of magnetic levitation systems via energy balancing," *in Proceedings American Control Conference*, 2000.

[26] J. Ferguson, R. H. Middleton, and A. Donaire, "Disturbance rejection via control by interconnection of port-Hamiltonian systems," in *2015 54th IEEE Conference on Decision and Control (CDC)*, Dec 2015, pp. 507–512.

[27] J. Tomassini, A. Donaire, S. Junco, and T. Perez, "A port-Hamiltonian approach to exponential stabilisation and disturbance rejection of a DC-DC buck converter with a nonlinear load," in *2017 11th Asian Control Conference (ASCC)*, Dec 2017, pp. 132–137.

[28] S. Knorn, A. Donaire, J. C. Agüero, and R. H. Middleton, "Passivity-based control for multi-vehicle systems subject to string constraints," *Automatica*, vol. 50, no. 12, pp. 3224 – 3230, 2014.

[29] X. Litrico and V. Fromion, *Modeling and Control of Hydrosystems*, 01 2009.

[30] H. Y. Cao and N. Deng, "Design of water tank level cascade control system based on siemens S7-200," in *2016 IEEE 11th Conference on Industrial Electronics and Applications (ICIEA)*, June 2016, pp. 1926–1928.

[31] J. Vojtesek and P. Dostal, "Adaptive control of water level in real model of water tank," in *2015 20th International Conference on Process Control (PC)*, June 2015, pp. 308–313.

[32] V. Dalmas, G. Robert, C. Poussot-Vassal, I. P. Duff, and C. Seren, "From infinite dimensional modelling to parametric reduced-order approximation: Application to open-channel flow for hydroelectricity," in *2016 European Control Conference (ECC)*, June 2016, pp. 1982–1987.

[33] H. A. Nasir, M. Cantoni, and E. Weyer, "An efficient implementation of Stochastic MPC for open channel water-level planning," in *2017 IEEE 56th Annual Conference on Decision and Control (CDC)*, Dec 2017, pp. 511–516.

[34] N. Zeng, L. Cen, and D. Li, "Distributed model predictive control for a multi-reach open-channel system," in *2017 11th Asian Control Conference (ASCC)*, Dec 2017, pp. 917–922.

[35] V. Dalmas, G. Robert, G. Besançon, and D. Georges, "Saint-Venant Reduced Order Model for Water Level Control in Open Channels," in *2018 IEEE Conference on Decision and Control (CDC)*, Dec 2018, pp. 7158–7163.

[36] R. M. Alarcón, O. A. Briones, N. E. Cisneros, M. A. Suárez, and A. J. Rojas, "Micro-velocimeter for an open channel flow: a simple and economical alternative," in *2019 IEEE CHILEAN Conference on Electrical, Electronics Engineering, Information and Communication Technologies (CHILECON)*, Nov 2019, pp. 1–6.

[37] L. A. Mora, J. I. Yuz, H. Ramirez, and Y. L. Gorrec, "A port-Hamiltonian Fluid-Structure Interaction Model for the Vocal folds." in *6th IFAC Workshop on Lagrangian and Hamiltonian Methods for Nonlinear Control LHMNC 2018*, 2018, pp. 62 – 67.

[38] N. Cisneros, H. Ramírez, and A. J. Rojas, "Port Hamiltonian modelling and control of a micro-channel," in *2019 Australian New Zealand Control Conference (ANZCC)*, Nov 2019, pp. 82–87.

[39] Y. Wang, C. Li, and C. Tian, "Modified recursive least squares algorithm for sparse system identification," in *2015 7th International Conference on Modelling, Identification and Control (ICMIC)*, Dec 2015, pp. 1–5.

[40] R. Valarmathi and M. Guruprasath, "System identification for a MIMO process," in *2017 International Conference on Computation of Power, Energy Information and Commuincation (ICCPEIC)*, March 2017, pp. 435–441.

[41] B. Raafiu and P. A. Darwito, "Identification of Four Wheel Mobile Robot based on Parametric Modelling," in *2018 International Seminar on Intelligent Technology and Its Applications (ISITIA)*, Aug 2018, pp. 397–401.

[42] A. Miller, "Identification of a multivariable incremental model of the vessel," in *2016 21st International Conference on Methods and Models in Automation and Robotics (MMAR)*, Aug 2016, pp. 218–224.

[43] P. Burrascano, S. Laureti, L. Senni, G. Silipigni, R. Tomasello, and M. Ricci, "Chirp design in a pulse compression procedure for the identification of non-linear systems," in *2017 14th International Conference on Synthesis, Modeling, Analysis and Simulation Methods and Applications to Circuit Design (SMACD)*, June 2017, pp. 1–4.

[44] U. Ahmad, M. Ahsan, A. I. Qazi, and M. A. Choudhry, "Modeling of lateral dynamics of a UAV using system identification approach," in *2015 International Conference on Information and Communication Technologies (ICICT)*, Dec 2015, pp. 1–5.

[45] B. Hamroun, "Approche hamiltonienne à ports pour la modélisation, la réduction et la commande des systèmes non linéaires à paramètres distribués : application aux écoulements à surface libre," vol. 1, 2009.

[46] J. P. Norton, *An Introduction to Identification*. New York, NY, USA: Dover Publications, Inc., 2009.

[47] R. M. Alarcón, O. A. Briones, O. Link, and A. J. Rojas, "Reproduction of hydrographs in a micro-canal, through the design of a decentralized PPI control for a TITO model," in *2018 IEEE International Conference on Automation/XXIII Congress of the Chilean Association of Automatic Control (ICA-ACCA)*, Oct 2018, pp. 1–6.

[48] R. Ortega and E. García-Canseco, "Interconnection and Damping Assignment Passivity-Based control: A survey," *European Journal of Control*, vol. 10, no. 5, pp. 432 – 450, 2004.

[49] A. Donaire and S. Junco, "On the addition of integral action to port-controlled Hamiltonian systems," *Automatica*, vol. 45, no. 8, pp. 1910 – 1916, 2009.

[50] R. Ortega and J. G. Romero, "Robust integral control of port-Hamiltonian systems: The case of non-passive outputs with unmatched disturbances," in *2011 50th IEEE Conference on Decision and Control and European Control Conference*, Dec 2011, pp. 3222–3227.

[51] Y. R. Teo, A. Donaire, and T. Perez, "Regulation and integral control of an underactuated robotic system using IDA-PBC with dynamic extension," in *2013 IEEE/ASME International Conference on Advanced Intelligent Mechatronics*, July 2013, pp. 920–925.

[52] S. Aranovskiy, R. Ortega, and R. Cisneros, "Robust PI passivity-based control of nonlinear systems: Application to port-Hamiltonian systems and temperature regulation," in *2015 American Control Conference (ACC)*, July 2015, pp. 434–439.

[53] M. Ryalat, D. S. Laila, and M. M. Torbati, "Integral IDA-PBC and PID-like control for port-controlled Hamiltonian systems," in *2015 American Control Conference (ACC)*, July 2015, pp. 5365–5370.

[54] J. Ferguson, A. Donaire, and R. H. Middleton, "Integral Control of Port-Hamiltonian Systems: Nonpassive Outputs Without Coordinate Transformation," *IEEE Transactions on Automatic Control*, vol. 62, no. 11, pp. 5947–5953, Nov 2017.

[55] M. Zhang, P. Borja, R. Ortega, Z. Liu, and H. Su, "PID Passivity-Based Control of Port-Hamiltonian Systems," *IEEE Transactions on Automatic Control*, vol. 63, no. 4, pp. 1032–1044, April 2018.

[56] F. Zhuang and Y. Huang, "Integral control in the current loop of permanent magnet synchronous motor based on passivity," in *2017 Chinese Automation Congress (CAC)*, Oct 2017, pp. 1181–1186.

[57] Y. Meng, S. Shang, H. Zhang, Y. Cui, and X. Wang, "IDA-PB control with integral action of Y-connected modular multilevel converter for fractional frequency transmission application," *IET Generation, Transmission Distribution*, vol. 12, no. 14, pp. 3385–3397, 2018.

[58] N. Khefifi, A. Houari, M. Ait-Ahmed, M. Machmoum, and M. Ghanes, "Robust IDA-PBC Based Load Voltage Controller for Power Quality Enhancement of Standalone Microgrids," in *IECON 2018 - 44th Annual Conference of the IEEE Industrial Electronics Society*, Oct 2018, pp. 249–254.